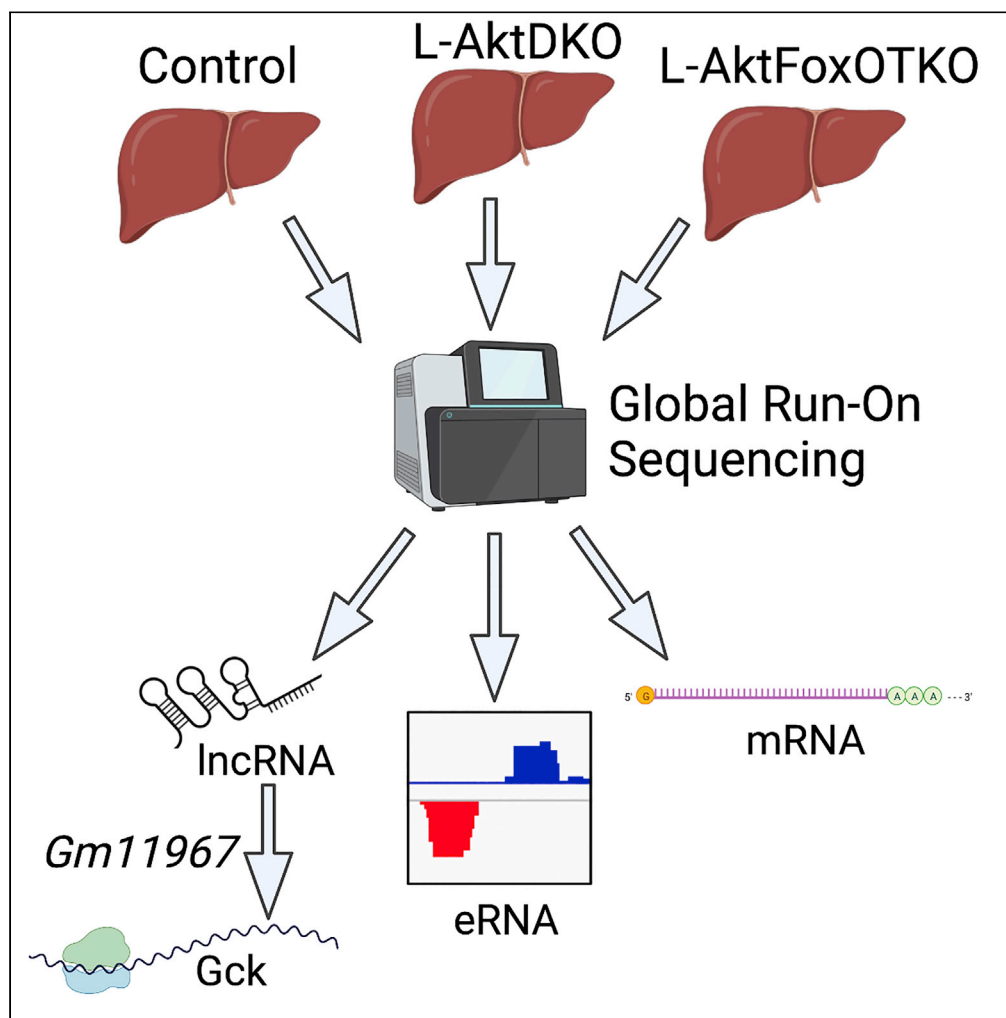


Article

Global-run on sequencing identifies *Gm11967* as an Akt-dependent long noncoding RNA involved in insulin sensitivity

Dominic Santoleri,
Hee-Woong Lim,
Matthew J.
Emmett, ..., Kathy
Fange Liu,
Mitchell A. Lazar,
Paul M. Titchenell

ptitc@penmedicine.upenn.
edu

Highlights

The hepatic
transcriptional
response to
nutrients was
determined by GRO-seq

The role of Akt/FoxO1
on feeding-dependent
nascent transcripts was
characterized

The lncRNA, *Gm11967*,
was identified as a
translational regulator of
glucokinase

Santoleri et al., iScience 25,
104410
June 17, 2022 © 2022 The
Author(s).
[https://doi.org/10.1016/
j.isci.2022.104410](https://doi.org/10.1016/j.isci.2022.104410)

Article

Global-run on sequencing identifies *Gm11967* as an Akt-dependent long noncoding RNA involved in insulin sensitivity

Dominic Santoleri,^{1,2,9} Hee-Woong Lim,^{3,4,9} Matthew J. Emmett,⁵ Julian Stoute,^{1,6} Matthew J. Gavin,² Jaimarie Sostre-Colón,² Kahealani Uehara,^{1,2} Jaclyn E. Welles,² Kathy Fange Liu,^{1,6} Mitchell A. Lazar,^{2,7} and Paul M. Titchenell^{1,2,8,10,*}

SUMMARY

The insulin responsive Akt and FoxO1 signaling axis is a key regulator of the hepatic transcriptional response to nutrient intake. Here, we used global run-on sequencing (GRO-seq) to measure the nascent transcriptional response to fasting and refeeding as well as define the specific role of hepatic Akt and FoxO1 signaling in mediating this response. We identified 599 feeding-regulated transcripts, as well as over 6,000 eRNAs, and mapped their dependency on Akt and FoxO1 signaling. Further, we identified several feeding-regulated lncRNAs, including the lncRNA *Gm11967*, whose expression was dependent upon the liver Akt-FoxO1 axis. Restoring *Gm11967* expression in mice lacking liver Akt improved insulin sensitivity and induced glucokinase protein expression, indicating that Akt-dependent control of *Gm11967* contributes to the translational control of glucokinase. More broadly, we have generated a unique genome-wide dataset that defines the feeding and Akt/FoxO1-dependent transcriptional changes in response to nutrient availability.

INTRODUCTION

The liver is an essential organ that regulates whole-body metabolism, storing, converting, and redistributing nutrients to meet the body's energetic demands (Rui, 2014). As the body transitions between feeding and fasting, the liver shifts between storing nutrients during nutrient surfeit and releasing them when they are scarce. Insulin is a key endocrine hormone responsible for regulating the liver's switch from fasting to feeding. The serine/threonine kinase Akt plays a central role in the hepatic response to insulin, promoting hepatic glucose utilization, glycogen synthesis, and lipogenesis while simultaneously suppressing gluconeogenesis (Titchenell et al., 2017; Santoleri and Titchenell, 2018). Hepatic deletion of both Akt1 and Akt2 (L-AktDKO), the two most abundant isoforms of Akt in the liver, causes hyperglycemia, insulin resistance, and defective glycogen and lipid synthesis, which confirm Akt's central role in mediating hepatic insulin action (Lu et al., 2012; Titchenell et al., 2016).

One of the key mechanisms by which insulin and Akt coordinate hepatic metabolism is by controlling gene transcription. Forkhead Box O1 (FoxO1) is a transcription factor that is directly phosphorylated and inhibited by Akt following insulin stimulation (Haeusler et al., 2014). Canonically, FoxO1 regulates hepatic glucose production by promoting gluconeogenesis (Matsumoto et al., 2007). FoxO1 inactivation alone is sufficient to reduce serum insulin levels and glucose tolerance under obesogenic insulin resistance (Altofonte et al., 2003; Samuel et al., 2006; Lu et al., 2012; Titchenell et al., 2016). Moreover, loss of FoxO1 in mice lacking hepatic Akt (L-AktFoxo1TKO) completely restores blood glucose and insulin sensitivity while largely normalizing the hepatic transcriptional response to feeding (Lu et al., 2012; O-Sullivan et al., 2015).

Although it is evident that insulin robustly changes the transcriptional state of the liver, the full extent of this response is still being clarified, and there have been several large-scale studies performed to understand how fasting, feeding, and insulin signaling regulate hepatic transcription at a global level. Global RNA profiling methods, such as RNA sequencing (RNA-seq) and microarray gene expression analysis, have shed light on many of the transcriptional processes that are regulated by insulin or feeding and have proven

¹Biochemistry and Molecular Biophysics Graduate Group, University of Pennsylvania Biomedical Graduate Studies, Philadelphia, PA 19104, USA

²Institute of Diabetes, Obesity and Metabolism, Smilow Center for Translational Research, University of Pennsylvania Perelman School of Medicine, 3400 Civic Center Blvd, Building 421, Philadelphia, PA 19104, USA

³Division of Biomedical Informatics, Cincinnati Children's Hospital Medical Center, Cincinnati, OH 45229, USA

⁴Department of Pediatrics, University of Cincinnati, Cincinnati, OH 45229, USA

⁵Department of Medicine, Massachusetts General Hospital, Boston, MA 02114, USA

⁶Department of Biochemistry and Biophysics, University of Pennsylvania Perelman School of Medicine, Philadelphia, PA 19104, USA

⁷Division of Endocrinology, Diabetes, and Metabolism, Department of Medicine, Perelman School of Medicine at the University of Pennsylvania, Philadelphia, PA 19104, USA

⁸Department of Physiology, University of Pennsylvania Perelman School of Medicine, Philadelphia, PA 19104, USA

⁹These authors contributed equally

¹⁰Lead contact

*Correspondence: ptitc@penmedicine.upenn.edu

<https://doi.org/10.1016/j.isci.2022.104410>



extremely useful in guiding scientific questioning (Yang et al., 2016; Fazakerley et al., 2018; Batista et al., 2019). For all of their benefits, the main drawback of these profiling techniques is that they do not directly measure changes in active transcription. Instead, these methods report cellular steady-state RNA content, which is determined by the combination of RNA transcription and RNA degradation. Unlike these other methods, global run-on sequencing (GRO-seq) measures nascent transcription of RNA, which allows for the direct assessment of active transcription in response to feeding and insulin without simultaneous changes in RNA degradation (Core et al., 2008).

Because GRO-seq measures nascent transcription as opposed to RNA levels, it can also be a powerful tool for detecting RNA transcripts that are normally lowly expressed or are only expressed transiently before being degraded (Lopes et al., 2017). As such, this technique is highly suited for measuring the expression of noncoding RNAs. Noncoding RNAs make up almost two-thirds of a cell's transcriptional load despite not coding for any protein. One of the largest classes of noncoding RNAs is long-noncoding RNAs (lncRNAs), which are at least 200 nucleotides long and often consist of two or more exons (Marques and Ponting, 2014). lncRNAs are understudied despite being associated with many human diseases, particularly cancers (Gupta et al., 2010; Batista and Chang, 2013) but also metabolic diseases including obesity (Dallner et al., 2019). lncRNAs are known to play many diverse roles in the cell, ranging from acting as transcription factors, to controlling mRNA stability, to acting as protein scaffolds (Zhang et al., 2019). Better understanding lncRNA function and regulation could provide critical insights into the transcriptional regulation of metabolism.

Here, we performed GRO-seq in fasted and refed mice as well as in L-AktDKO and AktFoxo1TKO mice to directly assess how feeding and insulin signaling control hepatic transcription, with a particular focus on changes in lncRNA expression. Although GRO-seq has previously been utilized to assess liver biology, such as how circadian rhythms alter liver metabolism (Guan et al., 2018; Fang et al., 2021) or cataloging the changes in transcription of hepatocytes during differentiation (Viiri et al., 2019), this is the first time that this technique has been used to measure transcriptional changes in fasting and refeeding and define the specific role of key insulin signaling mediators in modulating transcription. Using this method, we identified the lncRNA *Gm11967* as a highly feeding-dependent lncRNA that plays a role in controlling insulin sensitivity and hepatic glucokinase protein levels downstream of Akt signaling.

RESULTS

Akt plays a major role in feeding-induced nascent gene transcription in liver

Nutrient availability induces dramatic changes in liver through the action of insulin and other metabolites (Bideyan et al., 2021). In order to obtain a global view of these changes, we used GRO-seq to measure nascent RNA transcription in overnight fasted and 2-h refed control mice. Two independent GRO-seq experiments were performed for each condition, and the RPKM values averaged together. For both conditions, there was a high degree of correlation with a Pearson correlation coefficient of 0.8633 for the fasted replicates and 0.8058 for the 2-h refed replicates, indicating that the GRO-seq approach was quite robust across independent experiments (Figures S1A and S1B). Out of over 7,000 transcripts identified through this method, 599 were found to be differentially expressed between the two conditions; 279 were upregulated upon refeeding, whereas 320 were downregulated (Figure 1A).

Gene ontology (GO) analysis was performed on both sets of transcripts to determine which biological processes were most altered by refeeding (Figure 1B). Unsurprisingly, the biological processes most downregulated upon refeeding were those involved in fatty acid oxidation (Figure 1B), which included the acetyl-CoA dehydrogenases, *Acaadm* and *Acadl*, and acetyl-CoA oxidase (*Acox1*) that remove electrons from fatty acids for delivery into the electron transport chain (Swigoňová et al., 2009), as well as acetyl-CoA acyl transferase 2 (*Acaa2*), which catalyzes the last step of the fatty acid oxidation spiral, shortening the fatty acid tail (Bartlett and Eaton, 2004). Fatty acid oxidation is known to be suppressed by feeding and insulin (Muoio and Newgard, 2008). On the other hand, the pathways most upregulated by refeeding were those involved in the ER stress response (e.g. *Xbp1*, a transcription factor that gets alternatively processed during ER stress) (Calfon et al., 2002), insulin signaling pathways (e.g. *Igf1*, a key growth factor produced by the liver and promotes whole body metabolism) (Adamek and Kasprzak, 2018), and the growth hormone receptor (*Ghr*), which facilitates growth hormone action on the liver to promote metabolism (Dehkhoda et al., 2018).

To determine the specific role of hepatic insulin signaling in mediating these transcriptional changes, we generated L-AktDKO mice by injecting AAV8-TBG-CRE in *Akt1*^{loxP;loxP}; *Akt2*^{loxP;loxP} to inhibit the major

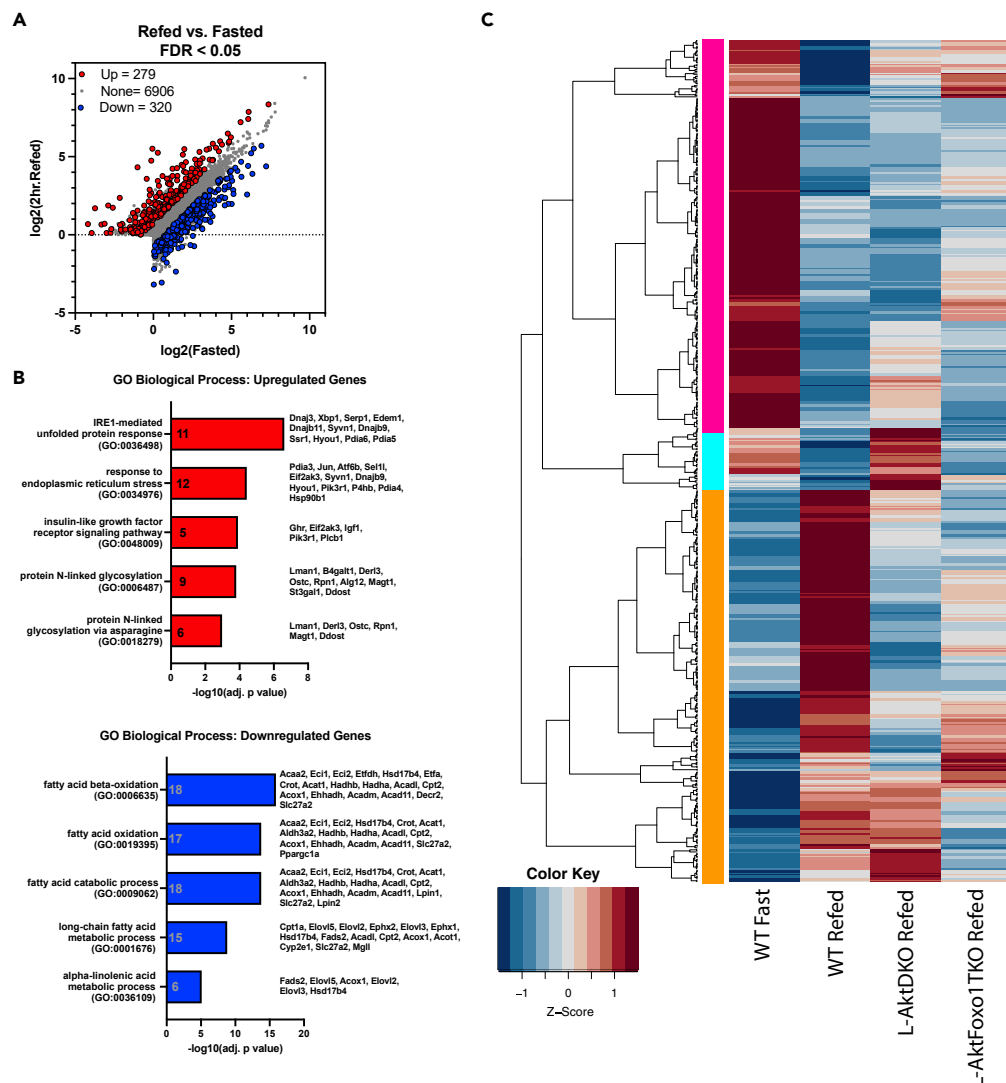


Figure 1. Feeding and the Akt pathway profoundly regulate hepatic gene transcription

(A) Scatterplot of GRO-seq results comparing nascent transcription in livers of overnight fasted mice with that of mice that were overnight fasted and then refed normal chow for 2 h. Genes with an RPKM over 1 that are significantly upregulated in refeeding with a false discovery rate less than 0.05 are highlighted in red, whereas downregulated genes with a false discovery rate less than 0.05 are highlighted in blue.

(B) Gene ontology performed on the sets of up- and downregulated genes identified by the GRO-seq analysis. The top five biological processes for each group are shown along with the respective genes that correlates with each process.

(C) Heatmap of all the feeding-regulated genes identified in (A) and further showing results of GRO-seq from 2-h refed L-AktDKO and L-AktFoxo1TKO mice. The two clusters correlate with genes that are downregulated (pink) or upregulated (orange) upon refeeding. The final cluster (cyan) are upregulated by refeeding as well as dependent upon Akt inhibition of FoxO1. Two known feeding/Akt-regulated genes, *Gck* and *IGFBP1*, are highlighted on the heatmap.

insulin responsive signal transduction cascade specifically in hepatocytes. The L-AktDKO mouse model has been extensively characterized and phenotyped in previous publications that document significant abnormalities in glucose and lipid metabolism (Lu et al., 2012; Titchenell et al., 2016). We performed similar GRO-seq analysis on 2-h refed L-AktDKO mice to assess the role of Akt signaling in regulating the liver's feeding response and compared the transcription profiles of the 599 genes identified to be differentially regulated by refeeding. Further, we performed a similar analysis in the L-AktFoxo1TKO mouse model, whereby FoxO1 is specifically deleted in the liver along with both Akt isoforms using the aforementioned AAV approach (Figure 1C). Notably, published work demonstrate that deletion of Foxo1 in Akt-deficient liver normalized glucose metabolism and partially restored some feeding-dependent transcriptional changes

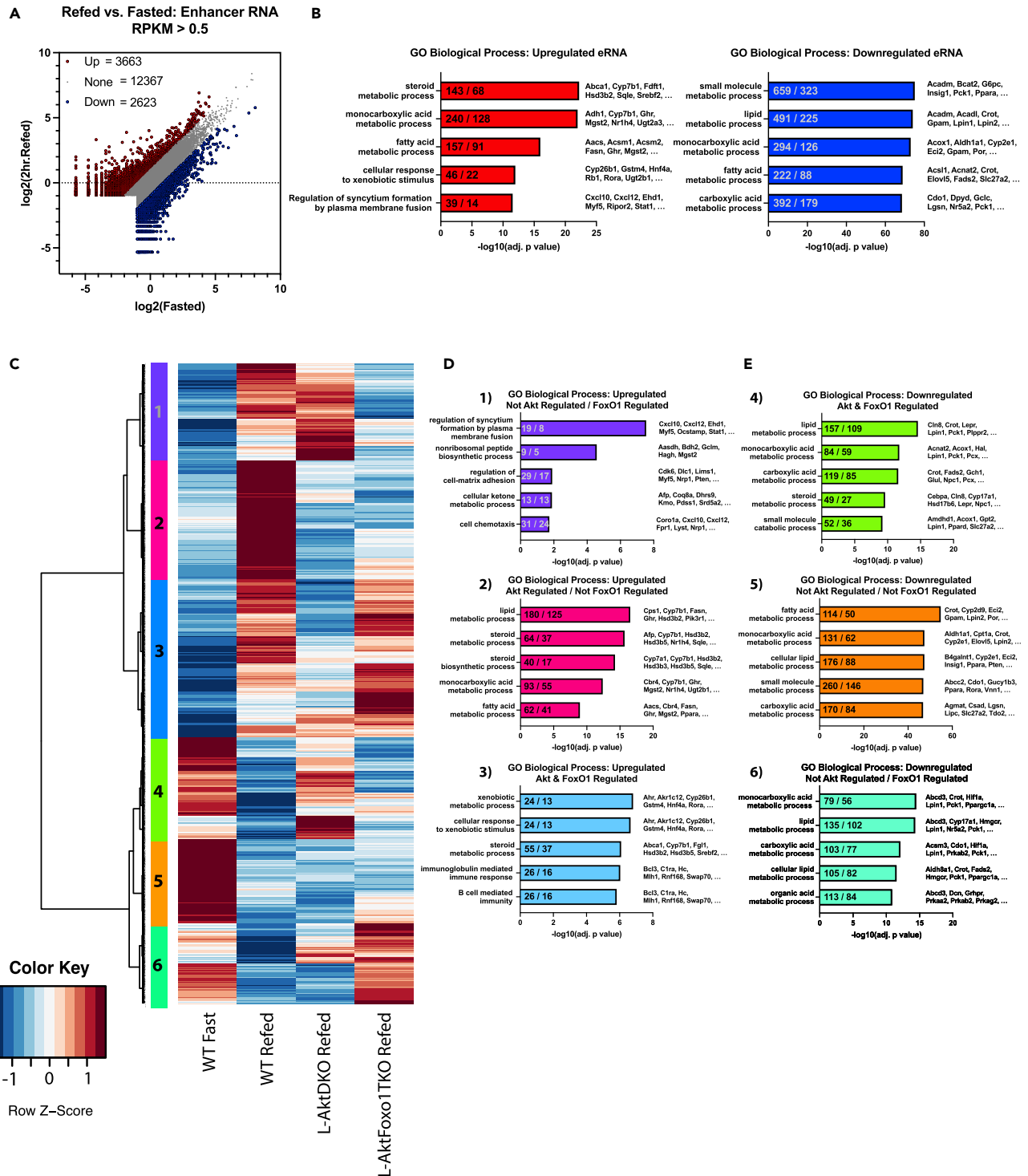


Figure 2. eRNA analysis of GRO-seq data demonstrates a complex system of gene regulation in response to refeeding and changes in Akt signaling

(A) Scatterplot of GRO-seq results comparing eRNA expression in livers of overnight fasted mice with that of mice that were overnight fasted and then refed normal chow for 2 h eRNA with an RPKM greater than 0.5 that are significantly upregulated in refeeding (at least 2-fold increased) are highlighted in red, whereas downregulated genes (at least 2-fold decreased) are highlighted in blue.

Figure 2. Continued

(B) GREAT gene ontology analysis performed on the sets of up- and downregulated genes identified by the GRO-seq analysis. The top five biological processes for each group are shown. Each process is represented by two values; the first represents the number of eRNAs identified within it and the second is the number of genes associated with those eRNAs within this pathway. Example genes are shown for each pathway.

(C) Heatmap of all the feeding-regulated genes identified in (A) and further results of GRO-seq from 2-h refed L-AktDKO and L-AktFoxo1TKO mice. Six clusters were identified, three from the feeding-stimulated eRNAs and three from the feeding-repressed that are differentially regulated by Akt and FoxO1.

(D) GREAT gene ontology analysis performed on the 3 clusters of feeding-stimulated eRNAs, identified by how they appear to be regulated by Akt and FoxO1. Each process is represented by two values, the first represents the number of eRNAs identified within it and the second is the number of genes associated with those eRNAs within this pathway. Example genes are shown for each pathway. Graph color corresponds to cluster in (C).

(E) GREAT gene ontology analysis performed on the 3 clusters of feeding-repressed eRNAs, identified by how they appear to be regulated by Akt and FoxO1. Each process is represented by two values; the first represents the number of eRNAs identified within it and the second is the number of genes associated with those eRNAs within this pathway. Example genes are shown for each pathway. Graph color corresponds to cluster in (C).

(Lu et al., 2012; Titchenell et al., 2016). A majority of the genes that were repressed upon refeeding were not affected by loss of Akt, indicating a majority of these nascent transcripts are regulated independently of Akt-FoxO1 (pink cluster Figure 1C). However, there were 40 feeding-suppressed genes that were induced upon Akt deletion and also normalized with concomitant deletion of FoxO1 (cyan cluster Figure 1C), suggesting that these are regulated through the Akt-FoxO1 axis. GO analysis of these genes found them to largely be genes involved in fatty acid metabolism and elongation (Figure S2A). One example from this subset is insulin-growth-factor-binding protein 1 (*Igfbp1*), which is more highly expressed during fasting and known to be FoxO1 dependent. FoxO1 ChIP-seq has previously demonstrated FoxO1 binding near *Igfbp1* (Kalvisa et al., 2018). GRO-seq showed *Igfbp1* expression increased in the L-AktDKO and was normalized with deletion of FoxO1 (Figures 1C and S2B).

On the other hand, most of the genes whose expression were induced upon refeeding were significantly decreased in L-AktDKO mice (orange cluster Figure 1C). Unlike the fasting-induced genes, the feeding-dependent genes affected by Akt deletion were only partially rescued with deletion of FoxO1 (Figure 1C). These data suggest that although much of Akt's capability to suppress fasting genes is dependent upon inhibition of FoxO1, FoxO1 suppression alone only partially controls the Akt-dependent feeding-induced genes. These genes include many known Akt targets including those involved in lipid metabolism. For example, *Gck*, a feeding dependent gene whose expression is known to be lost in the L-AktDKO, was only partially rescued following inhibition of FoxO1 (Figures 1C and S2C). As with *Igfbp1*, ChIP-seq has previously identified FoxO1 binding in close proximity to *Gck*, and additional work indicates that FoxO1 suppression of *Gck* occurs via the co-repressor Sin3a (Langlet et al., 2017; Kalvisa et al., 2018). Collectively, GRO-seq analysis of fasting and refed mouse liver identified several hundred nascent transcripts of known metabolically regulated processes. Moreover, many of the feeding-induced transcripts were dependent upon Akt signaling and partially controlled by FoxO1, suggesting both FoxO1-dependent and -independent pathways control hepatic transcription downstream of Akt signaling.

GRO-seq demonstrates that Akt and FoxO1 regulate enhancer RNA expression during fasting and refeeding

Because GRO-seq measures nascent transcription, it is an ideal method for detecting transiently expressed RNAs, such as enhancer RNAs (eRNAs) (Core et al., 2008; Core et al., 2014). Enhancer regions of the genome function similarly to promoter regions, acting as transcription factor binding sites to regulate expression of genes, although unlike promoters, enhancers are often kilobases or even megabases away from their target genes (Lam et al., 2014). When open, enhancer regions can be actively transcribed by RNA Pol II, creating eRNAs. These eRNAs are often small and quite transient, making them difficult to study, but they correlate strongly with active transcription; therefore, we mined our GRO-seq dataset to observe how enhancer activity changed with fasting and refeeding.

With our GRO-seq data, we identified over 18,000 eRNAs using a cutoff of RPKM >0.5. Among these eRNAs, the expression of 3,663 was induced at least 2-fold by feeding, whereas 2,623 were 2-fold repressed (Figure 2A). Taking these differentially expressed eRNAs, we used Genomic Regions Enrichment of Annotations Tool (GREAT) to assign putative target genes to each of them (McLean et al., 2010) and found classic feeding-responsive genes, such as *Srebfl1*, a feeding-induced, Akt-dependent transcription factor that promotes expression of lipogenic genes (Figure S3A), and *Pck1*, a key FoxO1-dependent gene involved in gluconeogenesis and known to be feeding-repressed through Akt signaling (Figure S3B). We further used the GREAT software to perform ontology analysis to determine what metabolic pathway changes

were correlated with the genes associated with the eRNAs. Although the feeding-repressed eRNAs represented many similar pathways as the repressed genes, fatty acid and small molecule metabolism as examples, the feeding-induced eRNAs did not correlate as strongly with the ER stress and unfolded protein response pathways as the feeding-induced nascent transcripts did (Figure 2B). Instead, metabolic pathways such as the steroid and monocarboxylic acid metabolic process were the most upregulated; this suggests ER stress is induced more acutely upon insulin signaling and enhancer activation related to fatty acid metabolic pathways follows for a sustained response.

We next explored how these feeding-regulated eRNAs were controlled in the L-AktDKO and L-AktFoxo1TKO mouse models by hierarchical clustering analysis. Both the feeding-induced and -repressed eRNAs each clustered into three distinct groups (Figure 2C). The majority of the feeding-induced eRNAs were dependent upon Akt for their induction (Figure 2C; clusters 2 and 3), with a slight majority of those requiring inhibition of FoxO1 for expression (cluster 3) while the rest were FoxO1 independent (cluster 2). Intriguingly, the last group from the feeding-induced eRNAs (Figure 2C; cluster 1), the Akt-independent eRNAs, all appeared to be dependent on FoxO1 activity in that loss of FoxO1 reduced their expression. During feeding, Akt classically inhibits FoxO1 activity, making this cluster of eRNAs that are induced by FoxO1 upon refeeding quite unique. Gene ontology for these three clusters revealed that the two Akt-dependent clusters were more enriched in metabolic pathways such as steroid and lipid metabolism, but this was much more prevalent in the cluster that did not require FoxO1. These results are unsurprising, as it is already known that loss of FoxO1 is not sufficient to restore Akt-dependent lipogenesis; concomitant activation of mTORC1 is also required (Titchenell et al., 2016). The Akt/FoxO1-dependent cluster had a greater representation of immune response pathways. Lastly, there were few metabolic pathways represented in the Akt-independent cluster, and instead, there were several pathways involved in cell motility and membrane structure, suggesting that FoxO1 may regulate these pathways via an Akt-independent mechanism (Figure 2D).

On the other hand, out of the feeding-repressed eRNAs, less than half were dependent upon Akt (Figure 2C; clusters 4, 5, and 6). This pattern is similar to the genes presented in Figure 1, with most of the feeding-induced genes being dependent upon Akt while the majority of feeding-repressed were Akt-independent. The Akt-independent eRNAs from the feeding-repressed group also split into two clusters depending on whether their repression was dependent upon FoxO1 (Figure 2C; clusters 5 and 6). Gene ontology for all three of these clusters showed very similar pathways being regulated, all related to metabolic pathways (Figure 2D). Similar to the nascent gene analysis, the feeding-repressed eRNA clusters had stronger representation of classic metabolism regulation than the feeding-induced ones, suggesting, perhaps, that feeding and insulin regulation of eRNAs play a stronger role in suppressing fasting metabolic pathways than promoting feeding ones.

Nascent RNA profiling identified *Gm11967* as a feeding and Akt-regulated lncRNA

lncRNAs play vital roles in regulating a diverse range of cellular functions yet remain understudied due to a lack of tools sensitive enough to functionally characterize them (Minati et al., 2021). As with eRNAs, GRO-seq is a powerful tool for identifying lncRNAs, and so we used this approach to detect feeding- and Akt-regulated lncRNAs. In order to investigate the lncRNAs that are feeding-regulated in the liver, we filtered the GRO-seq dataset to only include transcripts of annotated lncRNAs in Gencode. We identified 396 transcribed lncRNAs using this approach, of which 12 were significantly upregulated upon a 2-h refeed compared with an overnight fast, whereas 25 were downregulated (Figure 3A). Out of these differentially expressed lncRNAs, *Gm16551* and *Gm15441* were the most dramatically up- and downregulated, respectively. Previous work identified *Gm16551* as a target of sterol regulatory element binding protein 1c (SREBP1c), whereupon it induces a negative feedback loop to suppress SREBP1c activity (Yang et al., 2016). *Gm15441* was previously identified by RNA-seq as a fasting-induced gene that contributes to the hepatic inflammatory response (Batista et al., 2019; Brocker et al., 2020). Since these lncRNAs had previously been characterized, we focused on *Gm11967*, another lncRNA that was strongly induced by feeding in our GRO-seq dataset. Notably, *Gm11967* shares a promoter region with the hepatic isoform of glucokinase (*Gck*), a highly insulin- and Akt-dependent gene (Figure S4).

Consistent with *Gm11967* being a feeding-induced lncRNA, the expression of *Gm11967* is significantly reduced in L-AktDKO and is partially restored in the L-AktFoxo1TKO (Figure 3B). Notably, this expression pattern closely paralleled the transcriptional control of *Gck*, suggesting that the two transcripts could be

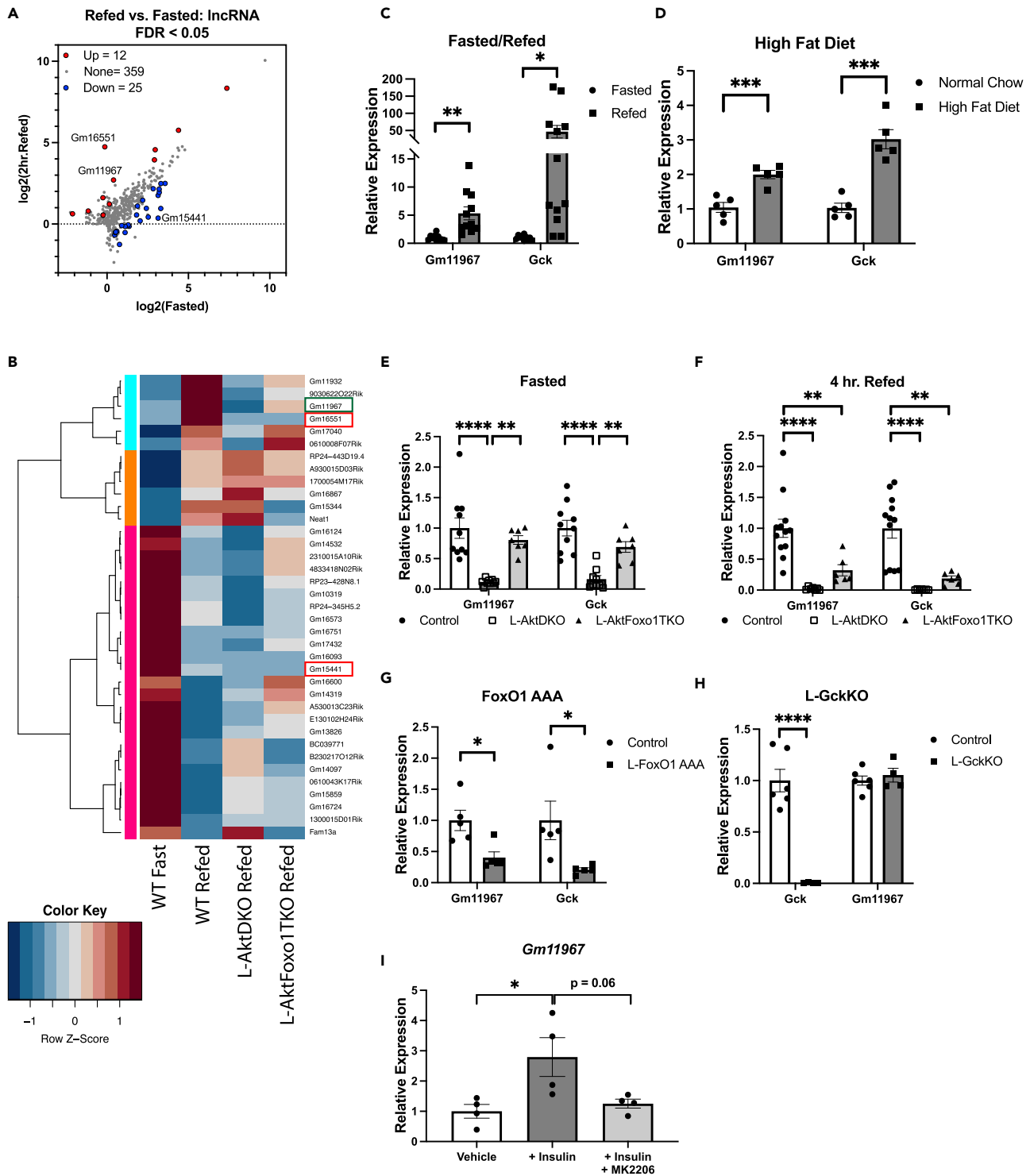


Figure 3. Identification of feeding and Akt-dependent lncRNAs by GRO-seq

(A) Scatterplot of all Gencode lncRNAs that were identified by GRO-seq in 16 h overnight fasted and 16 h overnight fasted then 2-h refed mice. lncRNAs that are upregulated in refeeding with a false discovery rate less than 0.05 are highlighted in red, whereas downregulated lncRNAs with a false discovery rate less than 0.05 are highlighted in blue. *Gm11967* is boxed in green, whereas *Gm16551* and *Gm15441* are boxed in red.

Figure 3. Continued

- (B) Heatmap of the 37 feeding-regulated lncRNAs and further comparison of their expression in 2-h refed L-AktDKO and L-AktFoxo1TKO mice. These data were grouped into three clusters; pink represents genes downregulated by refeeding, cyan represents feeding-induced, Akt-dependent genes, and orange represents feeding-induced, Akt-independent genes. *Gm16551* and *Gm15441* are boxed in red, whereas *Gm11967* is highlighted in green.
- (C) qPCR analysis of *Gm11967* and *Gck* in overnight fasted and refed mice (fasted $n = 10$ and refed $n = 12$).
- (D) qPCR analysis of *Gm11967* and *Gck* in 12-week high-fat-diet-fed mice (normal chow $n = 5$ and high-fat diet $n = 5$).
- (E) qPCR analysis of *Gm11967* and *Gck* expression in 16-h overnight fasted L-AktDKO and L-AktFoxo1TKO mice (control $n = 10$, L-AktDKO $n = 9$, L-AktFoxo1TKO $n = 7$).
- (F) qPCR analysis of *Gm11967* and *Gck* expression in refed L-AktDKO and L-AktFoxo1TKO mice (control $n = 12$, L-AktDKO $n = 7$, L-AktFoxo1TKO $n = 6$).
- (G) qPCR analysis of *Gm11967* and *Gck* expression in refed L-FoxO1 AAA mice (control $n = 5$ and FoxO1 AAA $n = 5$).
- (H) qPCR analysis of *Gm11967* and *Gck* expression in refed L-GckKO mice (control $n = 6$ and L-GckKO $n = 4$).
- (I) qPCR analysis of *Gm11967* expression in primary hepatocytes treated with insulin and MK2206 ($n = 4$ for all conditions from hepatocytes isolated from two different mice). Data are represented as mean \pm SEM (C–I). Statistical significance was determined either using Student's *t* test (C, D, G, and H) or one-way ANOVA with Tukey's multiple comparison test (E, F, and I). * $p < 0.05$, ** $p < 0.01$, *** $p < 0.001$, **** $p < 0.0001$.

regulated by the same factors. Further, neither *Gm16551* nor *Gm15441*, the other two lncRNAs strongly regulated by fasting and refeeding, shared the same Akt/FoxO1 dependence that *Gm11967* demonstrated, suggesting they are regulated by Akt-Foxo1-independent pathways (Figure 3B). It is worth noting that *Gm16551* fell into the same cluster of six lncRNAs that were Akt-dependent, including *Gm11967*, but unlike *Gm11967*, *Gm16551* was not FoxO1 regulated; this is unsurprising because *Gm16551* is controlled by SREBP1c, which is not rescued following Foxo1 deletion in AKT-deficient liver (Titchenell et al., 2016).

To confirm our findings from the GRO-seq analysis, we performed RT-qPCR to monitor *Gm11967* under various physiological conditions. Similar to *Gck* expression, refeeding increased *Gm11967* expression, albeit not to the magnitude as *Gck* (Figure 3C). Moreover, 12 weeks of high-fat diet feeding increased both the expression of *Gm11967* and *Gck* in liver consistent with diet-induced hyperinsulinemia (Figure 3D). As demonstrated by GRO-seq, *Gm11967* expression was significantly downregulated in both fasted and refed L-AktDKO mice and rescued in the L-AktFoxo1TKO (Figures 3E and 3F). In the refed samples, L-AktFoxo1TKO only partially rescued *Gm11967* expression.

Next, we determined if FoxO1 activity was sufficient to repress *Gm11967* expression. Here, we utilized a mouse model of liver-specific constitutive FoxO1 activity where the Akt-dependent phosphorylation sites are mutated to prevent Akt-mediated phosphorylation and inhibition of FoxO1 (L-FoxO1 AAA) (Zhang et al., 2006; Sostre-Colón et al., 2021). Consistent with the role of FoxO1 in the direct regulation of *Gm11967*, L-FoxO1 AAA mice had reduced levels of *Gm11967* and *Gck* (Figure 3G). Lastly, because *Gm11967* and *Gck* share a transcriptional start site, we assessed *Gm11967* expression levels in mice lacking glucokinase specifically in hepatocytes (L-GckKO). Hepatic deletion of *Gck* did not affect *Gm11967* expression, suggesting that although the two transcripts are regulated by similar factors/conditions, expression of *Gm11967* is not dependent upon *Gck* (Figure 3H). To verify that feeding-induced expression of *Gm11967* is driven by insulin signaling, we isolated primary hepatocytes and treated them with insulin as well as the Akt inhibitor, MK2206. Insulin treatment caused a ~3-fold increase in *Gm11967* expression in hepatocytes, whereas concomitant treatment with MK2206 returned expression to baseline (Figure 3I). Collectively, these data indicate that *Gm11967* is a feeding-induced lncRNA that is regulated by insulin through the Akt-FoxO1 axis in a similar manner to hepatic glucokinase.

***Gm11967* overexpression does not affect lipid metabolism downstream of Akt signaling**

We sought to characterize the biological role of *Gm11967* in hepatic metabolism by creating an AAV containing *Gm11967* driven by the liver-specific thyroxine binding globulin promoter to ensure hepatocyte-specific expression. First, we examined mice overexpressing *Gm11967* in the fasted state, to examine the specific role of *Gm11967* under conditions where *Gm11967* is physiologically low. After a 16-h overnight fast, *Gm11967* expression in mice injected with the AAV-TBG-*Gm11967* was over 200-fold higher than control mice (Figure S5A). Despite significant overexpression of *Gm11967*, these mice did not show any significant change in blood glucose, body weight, or liver size (Figures S5B and S5C).

We initially focused on the role of peroxisome proliferator-alpha (*Ppara*) expression and target genes because previous research in primary hepatocytes suggested that *Gm11967* may regulate its expression (Batista et al., 2019). *Ppara* expression is typically high during fasting and suppressed upon refeeding (Kersten et al., 1999), so it is possible that *Gm11967* might play a role in suppressing *Ppara* as the liver

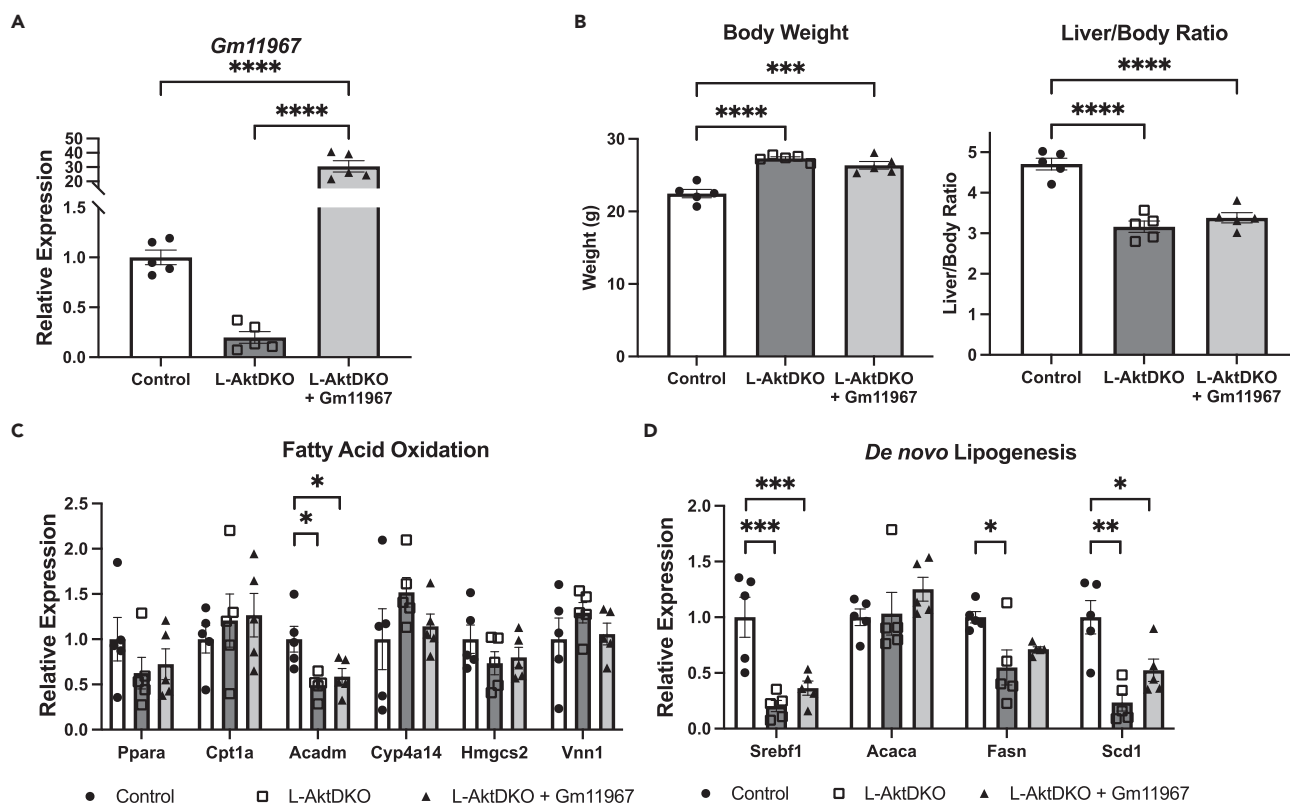


Figure 4. *Gm11967* overexpression does not affect lipid gene expression in L-AktDKO mice

(A) *Gm11967* expression levels in *ad libitum* fed control and L-AktDKO mice as well as L-AktDKO mice overexpressing *Gm11967* via a hepatocyte-specific AAV (for all conditions $n = 5$).

(B) Body weights of control, L-AktDKO, and *Gm11967* overexpressing L-AktDKO mice immediately after sacrificing along with the ratio of the liver weight to total body weight, represented as percentage of total body weight. Liver weight was recorded immediately after harvesting (for all conditions $n = 5$).

(C) mRNA expression levels of *Ppara* and several of its target genes involved in fatty acid oxidation in *ad libitum* fed control, L-AktDKO, and L-AktDKO + *Gm11967* mice (for all conditions $n = 5$).

(D) mRNA expression levels of genes involved in *de novo* lipogenesis in *ad libitum* fed control, L-AktDKO, and L-AktDKO + *Gm11967* mice (for all conditions $n = 5$). Data are represented as mean \pm SEM. Statistical significance was determined with an ordinary one-way ANOVA with Tukey's multiple comparison test. * $p < 0.05$, ** $p < 0.01$, *** $p < 0.001$, **** $p < 0.0001$.

transitions to a feeding state. However, overexpression of *Gm11967* in fasted mice did not alter the expression of *Ppara* or its target genes (Figure S5D). In addition to fatty acid oxidation genes, we also evaluated genes involved in *de novo* lipogenesis, another metabolic pathway regulated by Akt. Similar to genes involved in oxidation, we did not observe any major changes in the lipogenic genes in the fasted state with the exception of a mild increase in *Scd1* expression (Figure S5E). These data suggest that hepatic *Gm11967* overexpression does not play a significant role in the transcriptional control of *Ppara* or several other key Akt-regulated pathways in this model.

Because *Gm11967* expression is dependent upon Akt signaling, we explored the role of *Gm11967* in mice lacking hepatic Akt. This model enables us to measure the effects of overexpression during feeding, when *Gm11967* is normally expressed, without complications from endogenous *Gm11967* expression. Further, L-AktDKO mice exhibit increased fatty acid oxidation and decreased hepatic lipogenesis (Titchenell et al., 2016). Following AAV-*Gm11967* injection, we achieved high levels (~ 30 -fold above control expression and ~ 150 -fold higher than in normal L-AktDKO mice) of *Gm11967* in L-AktDKO mice 2 weeks postinjection (Figure 4A). Consistent with published reports, L-AktDKO mice demonstrated increased weight but decreased liver size, neither of which were affected by *Gm11967* overexpression (Figure 4B). First, we determined whether *Gm11967* overexpression affected *Ppara* expression or expression of its target genes involved in fatty acid oxidation based on the previous report for a role of *Gm11967* in *Ppara* regulation in isolated hepatocytes. *Gm11967* overexpression was not sufficient to alter expression of *Ppara* or its target

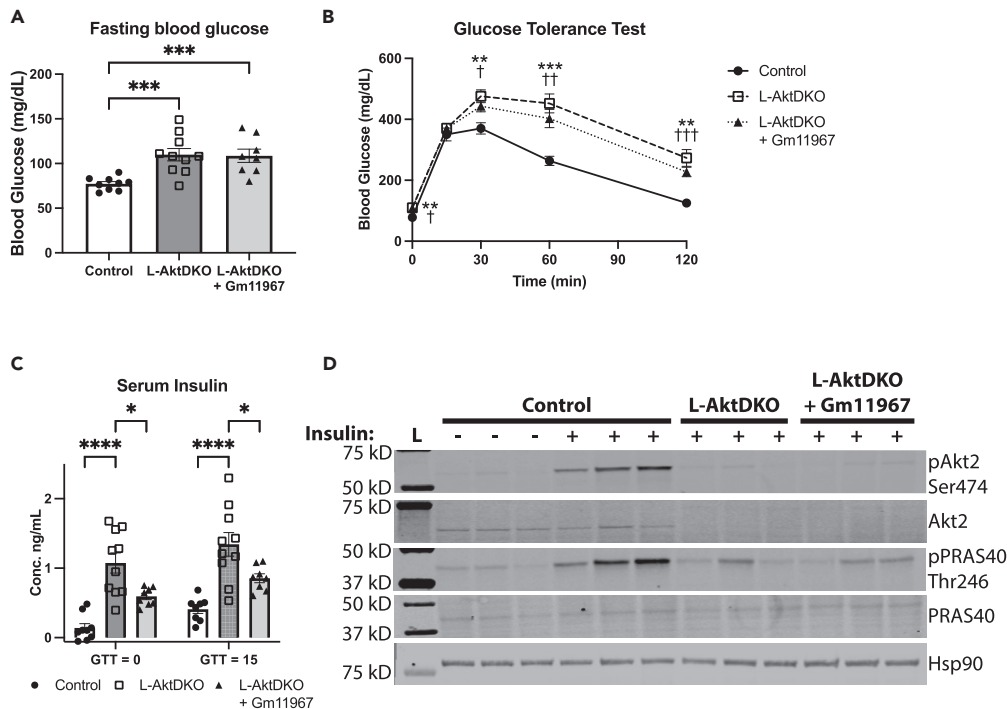


Figure 5. *Gm11967* partially rescues insulin sensitivity in L-AktDKO mice

(A) Blood glucose measurements of control, L-AktDKO, and L-AktDKO + *Gm11967* after a 16-h fast (control $n = 9$, L-AktDKO $n = 10$, L-AktDKO + *Gm11967* $n = 8$).
 (B) Intra-peritoneal glucose tolerance test performed on 16-h fasted control, L-AktDKO, and L-AktDKO + *Gm11967* (control $n = 8$, L-AktDKO $n = 10$, L-AktDKO + *Gm11967* $n = 8$).
 (C) Serum insulin levels of control, L-AktDKO, and L-AktDKO + *Gm11967* immediately prior to and 15 min into a glucose tolerance test (control $n = 8-9$, L-AktDKO $n = 10$, L-AktDKO + *Gm11967* $n = 8$).
 (D) Western blot analysis of phospho-Akt2 and phospho-PRAS40 in 16-h fasted control, L-AktDKO, and L-AktDKO + *Gm11967* that were injected with insulin for 20 min prior to sacrificing. Control mice not injected with insulin were used to compare insulin stimulation. Hsp90 was used as a loading control for all samples. ($n = 3$ for all conditions). Data are represented as mean \pm SEM (A–C). Statistical significance was determined with an ordinary one-way ANOVA with Tukey's multiple comparison test (A and C) or two-way ANOVA with Tukey's multiple comparison test (B). * $p < 0.05$, ** $p < 0.01$, *** $p < 0.001$, **** $p < 0.0001$.

genes in L-AktDKO mice (Figure 4C). Further, when we looked at other Akt-regulated lipid pathways, such as *de novo* lipogenesis, *Gm11967* overexpression did not rescue the expression of any of the lipogenic genes tested, including *Srebf1*, *Fasn*, and *Scd1* (Figure 4D).

***Gm11967* overexpression improves insulin resistance in L-AktDKO mice**

Although *Gm11967* overexpression did not affect lipid-related gene expression in L-AktDKO, we next wanted to determine if *Gm11967* controlled glucose homeostasis and insulin sensitivity, given the key role of Akt in these processes. Fasting blood glucose was increased in L-AktDKO mice and was not improved with *Gm11967* (Figure 5A). Further, overexpression of *Gm11967* in L-AktDKO did not improve glucose intolerance, which is known to worsen in the L-AktDKO model (Lu et al., 2012; Titchenell et al., 2015) (Figure 5B). However, both fasting and 15-min post-glucose-injection insulin levels were significantly lowered in L-AktDKO mice with *Gm11967* overexpression (Figure 5C). Although not sufficient to completely rescue insulin levels as that of FoxO1 deletion, these data show that *Gm11967* moderately improves insulin sensitivity in L-AktDKO mice.

To determine if these improvements of insulin sensitivity were associated with restored Akt signaling in L-AktDKO mice, we injected overnight fasted L-AktDKO with and without *Gm11967* with insulin for 20 min. As expected, there was no observable Akt2 phosphorylation in L-AktDKO or downstream Akt signaling (measured by phosphorylation of the direct Akt substrate PRAS40 at Thr246) (Figure 5D).

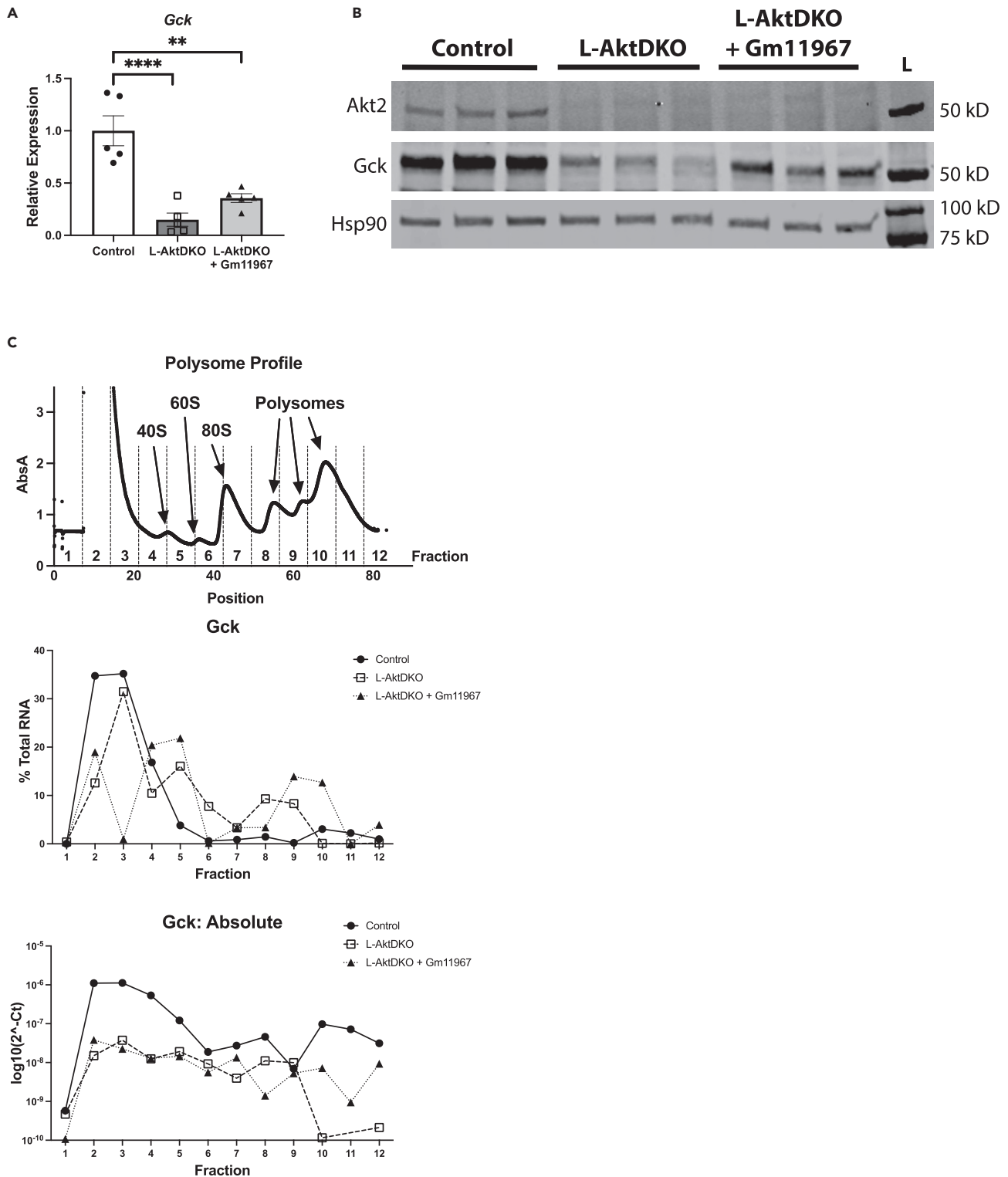


Figure 6. Gm11967 regulates hepatic Gck translation

(A) *Gck* mRNA expression levels in *ad libitum* fed control, L-AktDKO, and L-AktDKO + Gm11967 mice (for all conditions n = 5). Data are represented as mean ± SEM. Statistical significance was determined with an ordinary one-way ANOVA with Tukey's multiple comparison test. *p < 0.05, **p < 0.01, ***p < 0.001, ****p < 0.0001.

Figure 6. Continued

(B) Western blot analysis of Akt2 and Gck in *ad libitum* fed control, L-AktDKO, and L-AktDKO + Gm11967 (n = 3 for all conditions.). Hsp90 was used as a loading control.

(C) Polysome profiling on livers from control, L-AktDKO, and L-AktDKO + Gm11967 mice followed by RT-PCR on the fractions to determine Gck enrichment in each fraction. A representative profile (repeated n = 3) is depicted along with representative RT-PCR for each condition. Gck enrichment in each fraction is shown as both a percentage of total RNA in the sample as well as an absolute measure in each fraction.

Moreover, overexpression of *Gm11967* did not affect Akt signaling, as there was no detectable increase in Akt phosphorylation or the Akt target, PRAS40, in L-AktDKO mice with *Gm11967*. In addition, there was no significant difference in energy expenditure between L-AktDKO mice and those overexpressing *Gm11967*, as measured via CLAMS, suggesting no alterations in nutrient utilization (Figures S5F–S5H). These results show that *Gm11967* overexpression improves insulin sensitivity without restoring functional Akt signaling in liver or changing mouse energetics.

Gm11967 translationally upregulates Gck protein expression in L-AktDKO mice

Because many lncRNAs have been shown to regulate gene transcription in a variety of manners (Statello et al., 2021) and *Gm11967* shares a promoter region with *Gck* and is expressed under similar conditions, we hypothesized that *Gm11967* might control insulin sensitivity by regulating hepatic glucose homeostasis through regulation of *Gck*. We have previously reported that re-expression of *Gck* in L-AktDKO mice is sufficient to rescue insulin resistance and glucose tolerance (Titchenell et al., 2016). However, although *Gck* gene expression was reduced in the L-AktDKO, as expected, that reduction was not reversed following *Gm11967* overexpression (Figure 6A).

Although gene expression was not significantly changed by *Gm11967*, we observed a significant increase in hepatic Gck protein levels following overexpression of *Gm11967* in L-AktDKO mice, suggesting a potential posttranscriptional mechanism (Figure 6B). In order to investigate any potential changes in Gck translation, we performed polysome profiling on liver samples of L-AktDKO mice and those overexpressing *Gm11967* followed by RT-PCR to observe the degree of Gck RNA enrichment in the different polysome fractions changes. In the samples from L-AktDKO mice overexpressing *Gm11967*, there was a shift of Gck mRNA toward the heavier polysomal fractions as compared with the L-AktDKO samples, both as a measure of absolute RNA abundance or as a fraction of total Gck mRNA (Figure 6C); this demonstrates that Gck translation is more active with *Gm11967* overexpression in L-AktDKO, suggesting *Gm11967* regulates Gck translation downstream of Akt. Based on our previous data on Gck's effect on liver insulin sensitivity in the L-AktDKO model, this induction of Gck protein expression could in part explain the insulin-sensitizing effects that *Gm11967* has on the Akt-deficient liver.

DISCUSSION

Using GRO-seq to measure nascent transcription, we generated a robust dataset of the nascent transcriptional changes that occur in the liver in response to refeeding. This dataset is a useful resource for researchers interested in transcriptional regulations upon feeding or insulin action in the liver including nascent transcript, eRNA, and lncRNA information. In our manuscript, we found the biological pathways most repressed by 2-h refeeding after an overnight fast were those involved in fatty acid oxidation. It is well established that feeding and insulin repress fatty acid oxidation and that this repression is impaired in patients with type II diabetes (Hamel et al., 2001; Denis McGarry, 2002). Intriguingly the pathways most stimulated by 2-h of refeeding were those involved in ER stress and the unfolded protein response and not metabolic pathways such as *de novo* lipogenesis or protein synthesis. Previous studies have reported that feeding induces the ER stress response and that this plays key roles in normal glucose and lipid metabolism (Özcan et al., 2004; Sasako et al., 2019). These results build upon the idea that the ER stress response pathway plays a larger role in liver metabolism, particularly in the early stages of refeeding. At the eRNA level, feeding-repressed enhancers tracked very well with the repressed genes, with most of the identified pathways involved in fatty acid and carboxylic acid metabolism. Interestingly, the feeding-induced eRNAs did not have the same induction of ER stress pathways represented, suggesting perhaps that eRNA regulation of ER stress response occurs more acutely than 2 h. Instead, correlated regulation of eRNA and gene transcription were observed in the context of metabolic pathways in our data.

In addition, the GRO-seq dataset revealed many feeding-regulated lncRNAs. Several of the strongest hits, such as *Gm16551* and *Gm15441* have been identified as feeding-regulated and some of their function

already characterized, lending confidence to the results found in this dataset. We focused our attention on another highly feeding-dependent lncRNA, *Gm11967*, whose expression was regulated by the Akt-FoxO1 axis, unlike *Gm16551* and *Gm15441*. FoxO1 is known to bind near the *Gck* promoter region and regulate its activity. Noticeably, the binding site identified via ChIP-seq sits within *Gm11967*. Future studies should manipulate this region and see whether it regulates the feeding response of *Gm11967*.

A previous study investigating *Gm11967* demonstrated modest effects on *Ppar α* expression in isolated primary hepatocytes (Batista et al., 2019). In our hands, *Gm11967* overexpression *in vivo* did not affect *Ppar α* or expression of several of its target genes in fasted or L-AktDKO mice. However, it is quite possible that other facets of Akt signaling could be required for proper *Gm11967* regulation of *Ppar α* , thus meaning our model may not be capable of recapitulating this discovery and thus we cannot exclude *Ppar α* as a possible target of *Gm11967*.

We did discover that *Gm11967* was sufficient to partially normalize fasting and glucose-stimulated hyperinsulinemia classically seen in L-AktDKO mice. This improvement in insulin resistance correlated with increased translation of hepatic *Gck*. We have previously shown that overexpressing *Gck* is sufficient to normalize fasting serum insulin and glucose tolerance in L-AktDKO mice (Titchenell et al., 2016). It is possible that the overexpression of *Gm11967* in our model might result in altered activity of *Gm11967*. Despite this possibility, we feel the conclusion that *Gm11967* regulates hepatic insulin sensitivity through translational control of *Gck* to be fairly plausible, as the two genes are genomic neighbors and are expressed under very similar conditions. Further, *Gm11967* exerting its activity through *Gck* could also explain why *Gm11967* overexpression has little effect on fasting models, as *Gck* activity is suppressed during fasting both transcriptionally from lack of insulin (Matschinsky and Wilson, 2019) and catalytically through the action of glucokinase regulatory protein (GKRP) (De La Iglesia et al., 2000; Zelent et al., 2014).

To ascertain the precise mechanism by which *Gm11967* controls *Gck* translation, techniques such as ChIRP (Chromatin Isolation by RNA Purification) (Chu et al., 2011) and CHART (Capture Hybridization Analysis of RNA Targets) (Simon et al., 2011) are both powerful methods for studying lncRNA regulation of the genome and protein translation control (Cao et al., 2019). Future studies may employ these methods to investigate how *Gm11967* exerts its specific effect on *Gck* protein levels, the results of which could then be used to guide human studies. There is no known ortholog to *Gm11967* found in humans, but this is not surprising, as there is often very little sequence conservation in lncRNAs between species (Noviello et al., 2018). Functional characterization of *Gm11967* would enable identification of a human lncRNA that fulfills the same role of regulating *Gck* translation.

In conclusion, we used GRO-seq to generate an essential and unique genome-wide dataset outlining the feeding and Akt-dependent nascent transcriptional response in liver that will be of broad interest to the scientific community. Using this dataset, we further identified 37 feeding-dependent lncRNAs, of which 6 were shown to be Akt regulated. Using this dataset, we identified and characterized the feeding- and Akt-dependent gene, *Gm11967*, in the control of insulin sensitivity and *Gck* protein expression. Collectively, this study demonstrates how GRO-seq may serve as a powerful tool for identifying and prioritizing nascent transcripts and lncRNAs involved in various biological processes including the hepatic transcriptional response to nutrient intake.

Limitations of the study

A major limitation of our study regarding the *in vivo* role of *Gm11967* in the liver involves the use of an overexpression model. We utilized this approach in order to isolate the specific role of *Gm11967* as an Akt-dependent effector involved in the hepatic transcriptional response to nutrients. Imaging techniques such as RNA-FISH would be a useful to determine the cellular localization of endogenous and exogenous *Gm11967*. An alternative method to study *Gm11967* activity would be to reduce *Gm11967* expression via loss-of-function experiments. These experiments would further define the requirement of *Gm11967* in the hepatic transcriptional response and the translational control of glucokinase expression.

STAR★METHODS

Detailed methods are provided in the online version of this paper and include the following:

- KEY RESOURCES TABLE
- RESOURCE AVAILABILITY

- Lead contact
- Materials availability
- Data and code availability
- **EXPERIMENTAL MODEL AND SUBJECT DETAILS**
 - Mice
- **METHOD DETAILS**
 - GRO-seq
 - mRNA isolation and real-time PCR
 - Protein isolation and Western blotting
 - Glucose tolerance test
 - Serum insulin measurements
 - Primary hepatocyte isolation
 - Polysome profiling
- **QUANTIFICATION AND STATISTICAL ANALYSIS**

SUPPLEMENTAL INFORMATION

Supplemental information can be found online at <https://doi.org/10.1016/j.isci.2022.104410>.

ACKNOWLEDGMENTS

This work was supported by K01DK111715 (P.M.T.), R03122191 (P.M.T.), R01125497 (P.M.T.), and R35GM133721 (K.F.L.) institutional startup funds from the University of Pennsylvania (P.M.T.), Cox Research Institute, and the Samuel and Josephine Chiaffa Memorial Fund (P.M.T.). This work was also supported by Cincinnati Children's Research Foundation (Trustee Award and Center for Pediatric Genomics Award to H.L.). The Functional Genomics Core of the University of Pennsylvania is supported by the NIH Diabetes Research Center DK19525 (M.A.L.). The graphical abstract was created using [Biorender.com](https://biorender.com).

AUTHOR CONTRIBUTIONS

D.S. and P.M.T. were responsible for conceptualization, data analysis, and manuscript preparation. H.L. was involved in conceptualization, data analysis, and manuscript preparation. M.E., J.S., M.G., K.U., and J.S.-C. provided technical assistance. J.E.W. contributed to data analysis. K.F.L. and M.A.L. contributed to experimental design, data analysis, and data interpretation. P.M.T. directed the project. D.S. and P.M.T. wrote the manuscript with suggestions and comments provided by all authors.

DECLARATION OF INTERESTS

M.A.L. is an Advisory Board Member (Pfizer, Inc. and Flare, Inc.), recipient of grant funding unrelated to the present project (Pfizer, Inc.), and equity holder (Flare, Inc.). All other authors declare no competing interests.

Received: November 30, 2021

Revised: March 18, 2022

Accepted: May 11, 2022

Published: June 17, 2022

REFERENCES

- Adamek, A., and Kasprzak, A. (2018). Insulin-like growth factor (IGF) system in liver diseases. *Int. J. Mol. Sci.* 19, 1308. <https://doi.org/10.3390/ijms19051308>.
- Altomonte, J., Richter, A., Harbaran, S., Suriawinata, J., Nakae, J., Thung, S.N., Meseck, M., Accili, D., and Dong, H. (2003). Inhibition of Foxo1 function is associated with improved fasting glycemia in diabetic mice. *Am. J. Physiol. Endocrinol. Metab.* 285, E718–E728. <https://doi.org/10.1152/ajpendo.00156.2003>.
- Bartlett, K., and Eaton, S. (2004). Mitochondrial β -oxidation. *Eur. J. Biochem.* 271, 462–469. <https://doi.org/10.1046/j.1432-1033.2003.03947.x>.
- Batista, P.J., and Chang, H.Y. (2013). Long noncoding RNAs: cellular address codes in development and disease. *Cell* 152, 1298–1307. <https://doi.org/10.1016/j.cell.2013.02.012>.
- Batista, T.M., Garcia-Martin, R., Cai, W., Konishi, M., O'Neill, B.T., Sakaguchi, M., Kim, J.H., Jung, D.Y., Kim, J.K., and Kahn, C.R. (2019). Multi-dimensional transcriptional remodeling by physiological insulin in vivo. *Cell Rep.* 26, 3429–3443.e3. <https://doi.org/10.1016/j.celrep.2019.02.081>.
- Bideyan, L., Nagari, R., and Tontonoz, P. (2021). Hepatic transcriptional responses to fasting and feeding. *Genes Dev.* 35, 635–657. <https://doi.org/10.1101/GAD.348340.121>.
- Brocker, C.N., Kim, D., Melia, T., Karri, K., Velenosi, T.J., Takahashi, S., Aibara, D., Bonzo, J.A., Levi, M., Waxman, D.J., and Gonzalez, F.J. (2020). Long non-coding RNA Gm15441 attenuates hepatic inflammasome activation in response to PPARA agonism and fasting. *Nat. Commun.* 11, 5847. <https://doi.org/10.1038/s41467-020-19554-7>.
- Calfon, M., Zeng, H., Urano, F., Till, J.H., Hubbard, S.R., Harding, H.P., Clark, S.G., and Ron, D. (2002). Correction: corrigendum: IRE1

- couples endoplasmic reticulum load to secretory capacity by processing the XBP-1 mRNA. *Nature* 420, 202. <https://doi.org/10.1038/nature01193>.
- Cao, M., Zhao, J., and Hu, G. (2019). Genome-wide methods for investigating long noncoding RNAs. *Biomed. Pharmacother.* 2016, 395–401.
- Chen, E.Y., Tan, C.M., Kou, Y., Duan, Q., Wang, Z., Meirelles, G.V., Clark, N.R., and Ma'ayan, A. (2013). Enrichr: interactive and collaborative HTML5 gene list enrichment analysis tool. *BMC Bioinformatics* 14, 128. <https://doi.org/10.1186/1471-2105-14-128>.
- Chu, C., Qu, K., Zhong, F., Artandi, S., and Chang, H. (2011). Genomic maps of long noncoding RNA occupancy reveal principles of RNA-chromatin interactions. *Mol. Cell* 44, 667–678. <https://doi.org/10.1016/j.molcel.2011.08.027>.
- Core, L.J., Waterfall, J.J., and Lis, J.T. (2008). Nascent RNA sequencing reveals widespread pausing and divergent initiation at human promoters. *Science* 322, 1845–1848. <https://doi.org/10.1126/science.1162228>.
- Core, L.J., Martins, A.L., Danko, C.G., Waters, C.T., Siepel, A., and Lis, J.T. (2014). Analysis of nascent RNA identifies a unified architecture of initiation regions at mammalian promoters and enhancers. *Nat. Genet.* 46, 1311–1320. <https://doi.org/10.1038/ng.3142>.
- Dallner, O.S., Marinis, J.M., Lu, Y.H., Birsoy, K., Werner, E., Fayzikhodjaeva, G., Dill, B.D., Molina, H., Moscati, A., Kutalik, Z., et al. (2019). Dysregulation of a long noncoding RNA reduces leptin leading to a leptin-responsive form of obesity. *Nat. Med.* 25, 507–516. <https://doi.org/10.1038/s41591-019-0370-1>.
- De La Iglesia, N., Mukhtar, M., Seoane, J., Guinovart, J.J., and Agius, L. (2000). The role of the regulatory protein of glucokinase in the glucose sensory mechanism of the hepatocyte. *J. Biol. Chem.* 275, 10597–10603. <https://doi.org/10.1074/jbc.275.14.10597>.
- Dehkoda, F., Lee, C.M.M., Medina, J., and Brooks, A.J. (2018). The growth hormone receptor: mechanism of receptor activation, cell signaling, and physiological aspects. *Front. Endocrinol.* 9, 1–23. <https://doi.org/10.3389/fendo.2018.00035>.
- Denis McGarry, J. (2002). Banting lecture 2001. *Diabetes* 51, 7–18. <https://doi.org/10.2337/diabetes.51.1.7>.
- Emmett, M.J., Lim, H.W., Jager, J., Richter, H.J., Adlanmerini, M., Peed, L.C., Briggs, E.R., Steger, D.J., Ma, T., Sims, C.A., et al. (2017). Histone deacetylase 3 prepares Brown adipose tissue for acute thermogenic challenge. *Nature* 546, 544–548. <https://doi.org/10.1038/nature22819>.
- Fang, B., Everett, L., Jager, J., Briggs, E., Armour, S., Feng, D., Roy, A., Gerhart-Hines, Z., Sun, Z., and Lazar, M. (2014). Circadian enhancers coordinate multiple phases of rhythmic gene transcription in vivo. *Cell* 159, 1140–1152. <https://doi.org/10.1016/j.cell.2014.10.022>.
- Fang, B., Guan, D., and Lazar, M.A. (2021). Using GRO-seq to measure circadian transcription and discover circadian enhancers. *Methods Mol. Biol.* 2130, 127–148. https://doi.org/10.1007/978-1-0716-0381-9_10.
- Fazakerley, D.J., Chaudhuri, R., Yang, P., Maghzal, G.J., Thomas, K.C., Krycer, J.R., Humphrey, S.J., Parker, B.L., Fisher-Wellman, K.H., Meoli, C.C., et al. (2018). Mitochondrial CoQ deficiency is a common driver of mitochondrial oxidants and insulin resistance. *Elife* 7, 1–38. <https://doi.org/10.7554/eLife.32111>.
- Guan, D., Xiong, Y., Borck, P.C., Jang, C., Doulias, P.T., Papazyan, R., Fang, B., Jiang, C., Zhang, Y., Briggs, E.R., et al. (2018). Diet-induced circadian enhancer remodeling synchronizes opposing hepatic lipid metabolic processes. *Cell* 174, 831–842.e12. <https://doi.org/10.1016/j.cell.2018.06.031>.
- Gupta, R.A., Shah, N., Wang, K.C., Kim, J., Horlings, H.M., Wong, D.J., Tsai, M.C., Hung, T., Argani, P., Rinn, J.L., et al. (2010). Long non-coding RNA HOTAIR reprograms chromatin state to promote cancer metastasis. *Nature* 464, 1071–1076. <https://doi.org/10.1038/nature08975>.
- Haeusler, R.A., Hartil, K., Vaitheeswaran, B., Arrieta-Cruz, I., Knight, C.M., Cook, J.R., Kammoun, H.L., Febbraio, M.A., Gutierrez-Juarez, R., Kurland, I.J., and Accili, D. (2014). Integrated control of hepatic lipogenesis versus glucose production requires FoxO transcription factors. *Nat. Commun.* 5, 5190. <https://doi.org/10.1038/ncomms6190>.
- Hamel, F.G., Bennett, R.G., Upward, J.L., and Duckworth, W.C. (2001). Insulin inhibits peroxisomal fatty acid oxidation in isolated rat hepatocytes. *Endocrinology* 142, 2702–2706. <https://doi.org/10.1210/endo.142.6.8178>.
- Harrow, J., Denoeud, F., Frankish, A., Reymond, A., Chen, C.K., Chrast, J., Lagarde, J., Gilbert, J.G., Storey, R., Swarbreck, D., et al. (2006). GENCODE: producing a reference annotation for ENCODE. *Genome Biol.* 7, S4–S4.9. <https://doi.org/10.1186/gb-2006-7-s1-s4>.
- Kalvisa, A., Siersbæk, M.S., Præstholm, S.M., Christensen, L.J.L., Nielsen, R., Stohr, O., Vettorazzi, S., Tuckermann, J., White, M., Mandrup, S., and Grontved, L. (2018). Insulin signaling and reduced glucocorticoid receptor activity attenuate postprandial gene expression in liver. *PLoS Biol.* 16, e2006249. <https://doi.org/10.1371/journal.pbio.2006249>.
- Kersten, S., Seydoux, J., Peters, J.M., Gonzalez, F.J., Desvergne, B., and Wahli, W. (1999). Peroxisome proliferator-activated receptor α mediates the adaptive response to fasting. *J. Clin. Invest.* 103, 1489–1498. <https://doi.org/10.1172/JCI6223>.
- Kuleshov, M.V., Jones, M.R., Rouillard, A.D., Fernandez, N.F., Duan, Q., Wang, Z., Koplev, S., Jenkins, S.L., Jagodnik, K.M., Lachmann, A., et al. (2016). Enrichr: a comprehensive gene set enrichment analysis web server 2016 update. *Nucleic Acids Res.* 44, W90–W97. <https://doi.org/10.1093/nar/gkw377>.
- Lam, M.T.Y., Li, W., Rosenfeld, M.G., and Glass, C.K. (2014). Enhancer RNAs and regulated transcriptional programs. *Trends Biochem. Sci.* 39, 170–182. <https://doi.org/10.1016/j.tibs.2014.02.007>.
- Langlet, F., Haeusler, R.A., Linden, D., Ericson, E., Norris, T., Johansson, A., Cook, J.R., Aizawa, K., Wang, L., Buettner, C., and Accili, D. (2017). Selective inhibition of FOXO1 activator/repressor balance modulates hepatic glucose handling. *Cell* 171, 824–835.e18. <https://doi.org/10.1016/j.cell.2017.09.045>.
- Langmead, B., Trapnell, C., Pop, M., and Salzberg, S.L. (2009). Ultrafast and memory-efficient alignment of short DNA sequences to the human genome. *Genome Biol.* 10, R25. <https://doi.org/10.1186/gb-2009-10-3-r25>.
- Lopes, R., Agami, R., and Korkmaz, G. (2017). GRO-seq, A tool for identification of transcripts regulating gene expression. *Methods Mol. Biol.* 1543, 45–55.
- Lu, M., Wan, M., Leavens, K.F., Chu, Q., Monks, B.R., Fernandez, S., Ahima, R.S., Ueki, K., Kahn, C.R., and Birnbaum, M.J. (2012). Insulin regulates liver metabolism in vivo in the absence of hepatic Akt and Foxo1. *Nat. Med.* 18, 388–395. <https://doi.org/10.1038/nm.2686>.
- Marques, A.C., and Ponting, C.P. (2014). Intergenic lncRNAs and the evolution of gene expression. *Curr. Opin. Genet. Dev.* 27, 48–53.
- Martin, M. (2011). Cutadapt removes adapter sequences from high-throughput sequencing reads. *EMBnet.J.* 17, 10–12. <https://doi.org/10.14806/ej.17.1.200>.
- Matschinsky, F.M., and Wilson, D.F. (2019). The central role of glucokinase in glucose homeostasis: a perspective 50 years after demonstrating the presence of the enzyme in islets of langerhans. *Front. Physiol.* 10, 148. <https://doi.org/10.3389/fphys.2019.00148>.
- Matsumoto, M., Poci, A., Rossetti, L., DePinho, R.A., and Accili, D. (2007). Impaired regulation of hepatic glucose production in mice lacking the forkhead transcription factor Foxo1 in liver. *Cell Metab.* 6, 208–216. <https://doi.org/10.1016/j.cmet.2007.08.006>.
- McLean, C.Y., Bristol, D., Hiller, M., Clarke, S.L., Schaar, B.T., Lowe, C.B., Wenger, A.M., and Bejerano, G. (2010). GREAT improves functional interpretation of cis-regulatory regions. *Nat. Biotechnol.* 28, 495–501. <https://doi.org/10.1038/nbt.1630>.
- Minati, L., Firrito, C., Del Piano, A., Peretti, A., Sidoli, S., Peroni, D., Belli, R., Gandolfi, F., Romanel, A., Bernabo, P., et al. (2021). One-shot analysis of translated mammalian lncRNAs with AHARIBO. *Elife* 10, 1. <https://doi.org/10.7554/eLife.59303>.
- Muoio, D.M., and Newgard, C.B. (2008). Fatty acid oxidation and insulin action. *Diabetes* 57, 1455–1456. <https://doi.org/10.2337/db08-0281>.
- Noviello, T.M.R., Di Liddo, A., Ventola, G.M., Spagnuolo, A., D'Aniello, S., Ceccarelli, M., and Cerulo, L. (2018). Detection of long non-coding RNA homology, a comparative study on alignment and alignment-free metrics. *BMC Bioinformatics* 19, 407–412. <https://doi.org/10.1186/s12859-018-2441-6>.
- O'Sullivan, I., Zhang, W., Wasserman, D.H., Liew, C.W., Liu, J., Paik, J., DePinho, R.A., Stolz, D.B., Kahn, C.R., Schwartz, M.W., et al. (2015). FoxO1 integrates direct and indirect effects of insulin on

hepatic glucose production and glucose utilization. *Nat. Commun.* 6, 7079. <https://doi.org/10.1038/ncomms8079>.

Özcan, U., Cao, Q., Yilmaz, E., Lee, A.H., Iwakoshi, N.N., Özdelin, E., Tuncman, G., Görgün, C., Glimcher, L.H., and Hotamisligil, G.S. (2004). Endoplasmic reticulum stress links obesity, insulin action, and type 2 diabetes. *Science* 306, 457–461. <https://doi.org/10.1126/science.1103160>.

Postic, C., Shiota, M., Niswender, K.D., Jetton, T.L., Chen, Y., Moates, J.M., Shelton, K.D., Lindner, J., Cherrington, A.D., and Magnuson, M.A. (1999). Dual roles for glucokinase in glucose homeostasis as determined by liver and pancreatic β cell-specific gene Knock-outs using Cre recombinase. *J. Biol. Chem.* 274, 305–315. <https://doi.org/10.1074/jbc.274.1.305>.

Robinson, M.D., McCarthy, D.J., and Smyth, G.K. (2010). edgeR: a Bioconductor package for differential expression analysis of digital gene expression data. *Bioinformatics* 26, 139–140. <https://doi.org/10.1093/bioinformatics/btp616>.

Robinson, J.T., Thorvaldsdottir, H., Winckler, W., Guttman, M., Lander, E.S., Getz, G., and Mesirov, J.P. (2011). Integrative genomics viewer. *Nat. Biotechnol.* 29, 24–26. <https://doi.org/10.1038/nbt.1754>.

Rui, L. (2014). Energy metabolism in the liver. *Compr. Physiol.* 4, 177–197. <https://doi.org/10.1002/cphy.c130024>.

Samuel, V.T., Choi, C.S., Phillips, T.G., Romanelli, A.J., Geisler, J.G., Bhanot, S., McKay, R., Monia, B., Shutter, J.R., Lindberg, R.A., et al. (2006). Targeting Foxo1 in mice using antisense oligonucleotide improves hepatic and peripheral insulin action. *Diabetes* 55, 2042–2050. <https://doi.org/10.2337/db05-0705>.

Santoleri, D., and Titchenell, P.M. (2018). Resolving the paradox of hepatic insulin resistance. *Cell. Mol. Gastroenterol. Hepatol.* 447–456. <https://doi.org/10.1016/j.jcmgh.2018.10.016>.

Sasako, T., Ohsugi, M., Kubota, N., Itoh, S., Okazaki, Y., Terai, A., Kubota, T., Yamashita, S., Nakatsukasa, K., Kamura, T., et al. (2019). Hepatic Sdf211 controls feeding-induced ER stress and regulates metabolism. *Nat. Commun.* 10, 1–16. <https://doi.org/10.1038/s41467-019-08591-6>.

Simon, M.D., Wang, C.I., Kharchenko, P.V., West, J.A., Chapman, B.A., Alekseyenko, A.A., Borowsky, M.L., Kuroda, M.I., and Kingston, R.E. (2011). The genomic binding sites of a noncoding RNA. *Proc. Natl. Acad. Sci. U S A* 108, 20497–20502. <https://doi.org/10.1073/pnas.1113536108>.

Sostre-Colón, J., Uehara, K., Garcia Whitlock, A.E., Gavin, M.J., Ishibashi, J., Potthoff, M.J., Seale, P., and Titchenell, P.M. (2021). Hepatic AKT orchestrates adipose tissue thermogenesis via FGF21-dependent and -independent mechanisms. *Cell Rep.* 35, 109128. <https://doi.org/10.1016/j.celrep.2021.109128>.

Statello, L., Guo, C., Chen, L., and Huarte, M. (2021). Gene regulation by long non-coding RNAs and its biological functions. *Nat. Rev. Mol. Cell Biol.* 22, 96–118. <https://doi.org/10.1038/s41580-020-00315-9>.

Swigoňová, Z., Mohsen, A.W., and Vockley, J. (2009). Acyl-coA dehydrogenases: dynamic history of protein family evolution. *J. Mol. Evol.* 69, 176–193. <https://doi.org/10.1007/s00239-009-9263-0>.

Titchenell, P.M., Chu, Q., Monks, B.R., and Birnbaum, M.J. (2015). Hepatic insulin signalling is dispensable for suppression of glucose output by insulin in vivo. *Nat. Commun.* 6, 7078. <https://doi.org/10.1038/ncomms8078>.

Titchenell, P.M., Quinn, W.J., Lu, M., Chu, Q., Lu, W., Li, C., Chen, H., Monks, B.R., Chen, J., Rabinowitz, J.D., and Birnbaum, M.J. (2016). Direct hepatocyte insulin signaling is required for lipogenesis but is dispensable for the suppression of glucose production. *Cell Metabol.* 23, 1154–1166. <https://doi.org/10.1016/j.cmet.2016.04.022>.

Titchenell, P.M., Lazar, M.A., and Birnbaum, M.J. (2017). Unraveling the regulation of hepatic

metabolism by insulin. *Trends Endocrinol. Metab.* 28, 497–505. <https://doi.org/10.1016/j.tem.2017.03.003>.

Viiri, L.E., Rantapero, T., Kiamehr, M., Alexanova, A., Oittinen, M., Viiri, K., Niskanen, H., Nykter, M., Kaikkonen, M.U., and Aalto-Setälä, K. (2019). Extensive reprogramming of the nascent transcriptome during iPSC to hepatocyte differentiation. *Sci. Rep.* 9, 3562. <https://doi.org/10.1038/s41598-019-39215-0>.

Wang, D., Garcia-Bassets, I., Benner, C., Li, W., Su, X., Zhou, Y., Qiu, J., Liu, W., Kaikkonen, M.U., Ohgi, K.A., et al. (2011). Reprogramming transcription by distinct classes of enhancers functionally defined by eRNA. *Nature* 474, 390–394. <https://doi.org/10.1038/nature10006>.

Xie, Z., Bailey, A., Kuleshov, M.V., Clarke, D.J.B., Evangelista, J.E., Jenkins, S.L., Lachmann, A., Wojciechowicz, M.L., Kropiwnicki, E., Jagodnik, K.M., et al. (2021). Gene set Knowledge discovery with Enrichr. *Curr. Protoc.* 1, e90. <https://doi.org/10.1002/cpz1.90>.

Yang, L., Li, P., Yang, W., Ruan, X., Kiesewetter, K., Zhu, J., and Cao, H. (2016). Integrative transcriptome analyses of metabolic responses in mice define pivotal lncRNA metabolic regulators. *Cell Metab.* 24, 627–639. <https://doi.org/10.1016/j.cmet.2016.08.019>.

Zelent, B., Raimondo, A., Barrett, A., Buettger, C., Chen, P., Gloyn, A., and Matschinsky, F. (2014). Analysis of the co-operative interaction between the allosterically regulated proteins GK and GKRP using tryptophan fluorescence. *Biochem. J.* 459, 551–564. <https://doi.org/10.1042/BJ20131363>.

Zhang, W., Patil, S., Chauhan, B., Guo, S., Powell, D.R., Le, J., Klotsas, A., Matika, R., Xiao, X., Franks, R., et al. (2006). FoxO1 regulates multiple metabolic pathways in the liver. *J. Biol. Chem.* 281, 10105–10117. <https://doi.org/10.1074/jbc.M600272200>.

Zhang, X., Wang, W., Zhu, W., Dong, J., Cheng, Y., Yin, Z., and Shen, F. (2019). Mechanisms and functions of long non-coding RNAs at multiple regulatory levels. *Int. J. Mol. Sci.* 20, 5573. <https://doi.org/10.3390/ijms20225573>.

STAR★METHODS

KEY RESOURCES TABLE

REAGENT or RESOURCE	SOURCE	IDENTIFIER
<i>Antibodies</i>		
HSP90	Cell Signaling Technology	Cat# 4874; RRID: AB_2121214
AKT2	Cell Signaling Technology	Cat# 2964; RRID: AB_331162
P-AKT2 (Ser474)	Cell Signaling Technology	Cat# 8599; RRID: AB_26303478
P-PRAS40 (Thr246)	Cell Signaling Technology	Cat# 2997; RRID: AB_2258110
GCK	Gift from Magnuson Lab	N/A
PRAS40	Cell Signaling Technology	Cat# 2610; RRID: AB_916206
<i>Bacterial and virus strains</i>		
AAV8-TBG-CRE	University of Pennsylvania Vector Core	N/A
AAV8-TBG-eGFP	University of Pennsylvania Vector Core	N/A
AAV8-TBG-Gm11967	University of Pennsylvania Vector Core	N/A
<i>Biological samples</i>		
Murine Liver	This Paper	N/A
<i>Chemicals, peptides, and recombinant proteins</i>		
APE I	New England Biolabs	M0282
CirLigase	Epicentre	Cat# CL4111K
Collagenase Type 2	Worthington Biochemical	Cat# LS004174; CAS: 9001-12-1
Cycloheximide	Sigma-Aldrich	Cat# 1988; CAS: 66-81-9
DNase Vial (D2)	Worthington Biochemical	Cat# LK003172; CAS: 9003-98-9
Exonuclease I	Fermentas	EN0581
M-MuLV	New England Biolabs	Cat# M0253
MK2206	Toronto Research Chemicals	Cat# M425025
Novolin R (insulin human injection)	Novo Nordisk	Cat# 0169-1833-11; CAS: 9004-10-8
Pentobarbital	Sagent Pharmaceuticals	NDC: 25021-676-20; CAS: 76-74-4
Percoll	Cytiva	Cat# 17-0891-01
Phosphatase Inhibitor Cocktail 2	Sigma-Aldrich	Cat# P5726
Phosphatase Inhibitor Cocktail 3	Sigma-Aldrich	Cat# P0044
Phusion DNA Polymerase	New England Biolabs	Cat# M0530
Protease Inhibitor Cocktail Tablets	Roche	Cat# 04693159001
RNaseOut	Invitrogen	Cat# 10-777-019
Sarkosyl	Sigma-Aldrich	Cat# L9150; CAS: 97-78-9
Superase-In	Invitrogen	Cat# AM2694
SuperScript III One-Step RT-PCR System	Invitrogen	Cat# 12574-026
SYBR Green PCR Master Mix	Applied Biosystems	Cat# 43-687-02
TRizol	Invitrogen	Cat# 15596026
Trypan Blue	Gibco	Cat# 15-250-061; CAS: 72-57-1

(Continued on next page)

Continued		
REAGENT or RESOURCE	SOURCE	IDENTIFIER
Critical commercial assays		
Insulin ELISA	Crystal Chem	Cat# 90080
Pierce BCA Protein Assay Kit	Thermo Fisher Scientific	Cat# 23225
RNase-Free DNase Set	Qiagen	Cat# 79254
RNeasy Mini Kit	Qiagen	Cat# 74106
Deposited data		
Raw and analyzed GRO-seq data	This Paper	GEO: GSE189810
Experimental models: Cell lines		
Murine primary hepatocytes	This Paper	N/A
Experimental models: Organisms/strains		
Mouse/B6: Akt1 ^{loxp/loxp} ; Akt2 ^{loxp/loxp}	Lu et al., 2012	N/A
Mouse/B6: Akt1 ^{loxp/loxp} ; Akt2 ^{loxp/loxp} ; Foxo1 ^{loxp/loxp}	Lu et al., 2012	N/A
Mouse/B6: Foxo1AAA ^{loxp/loxp}	Zhang et al., 2006	N/A
Mouse/B6: Gck ^{loxp/loxp}	Postic et al., 1999	N/A
Mouse/B6: diet induced obese	Jackson Laboratories	Cat# 380050
Oligonucleotides		
See Table S1 for RT-PCR primers	N/A	N/A
Software and algorithms		
Bowtie	Langmead et al., 2009	http://bowtie-bio.sourceforge.net/index.shtml ; RRID: SCR_005476
EdgeR	Robinson et al., 2010	http://bioconductor.org/packages/edgeR/ ; RRID: SCR_012802
Enrichr	Icahn School of Medicine at Mount Sinai	https://maayanlab.cloud/Enrichr/ ; RRID: SCR_001575
Gencode	Harrow et al., 2006	https://www.gencodegenes.org/ ; RRID: SCR_014966
GREAT V4.0.4	Stanford University School of Medicine	http://great.stanford.edu/public/html/splash.php ; RRID: SCR_005807
Integrative Genomics Viewer V2.6.3	Broad Institute	https://software.broadinstitute.org/software/igv/ ; RRID: SCR_011793
Prism V9.3.1	GraphPad	https://www.graphpad.com/ ; RRID: SCR_002798
QuantStudio Software V1.4.2—for QuantStudio 5 Real-Time PCR Systems	Thermo Fisher	https://www.thermofisher.com/order/catalog/product/A28140?SID=srch-hj-A28140
RStudio 2021.09.2+382 "Ghost Orchid"	RStudio, PBC	https://www.rstudio.com/products/rstudio/ ; RRID: SCR_000432

RESOURCE AVAILABILITY

Lead contact

Further information about the protocols and requests for resources and reagents should be directed to and will be fulfilled by the lead contact, Paul M. Titchenell (ptitc@penmedicine.upenn.edu).

Materials availability

Mouse models and AAV viruses are available upon request.

Data and code availability

- GRO-seq data have been deposited into GEO and are publicly accessible as of the date of publication. Accession numbers are listed in the [key resources table](#).
- This paper does not report original code.
- Any additional data required to reanalyze the data reported here is available from the [lead contact](#) upon request.

EXPERIMENTAL MODEL AND SUBJECT DETAILS

Mice

All mice used in all experiments were male mice from the C57BL/6J background. The L-AktDKO, L-AktFoxo1TKO, L-FoxO1 AAA, and L-GckKO mice were described previously ([Postic et al., 1999](#); [Zhang et al., 2006](#); [Lu et al., 2012](#)). Mice were injected at 6–8 weeks of age with adeno-associated virus containing a liver-specific promoter, *thyroxine-binding globulin* (TBG), driving either GFP (AAV-GFP) or Cre (AAV-Cre) recombinase at a dose of 10^{11} genomic copies per mouse to generate wild-type (WT), L-AktDKO, L-AktFoxo1TKO. The Control group consisted of GFP-injected littermates floxed for the indicated genotypes. For *Gm11967* overexpression experiments, mice were injected with 5×10^{11} genomic copies of an AAV-TBG expressing *Gm11967* or AAV-GFP simultaneously with any AAV-GFP or AAV-Cre used to create genetic knockouts. Experiments were performed 2–3 weeks after virus injection. Diet-induced obese mice were obtained from Jackson Laboratories (380050) after 12 weeks on diet and continued on high fat diet for up to 3 weeks (Research Diets D12492i). Age matched mice on a chow diet were used as experimental controls. Mice were fasted for 5 hours before sacrificing. All mice experiments were reviewed and approved by the University of Pennsylvania Institutional Animal Care & Use Committee in accordance with the guidelines of the NIH.

METHOD DETAILS

GRO-seq

The nuclear run-on assay was performed from nuclei from fasted and 2-hour refeed mice and sequenced as described previously ([Fang et al., 2014](#); [Emmett et al., 2017](#)). Briefly, mouse livers were harvested following a 16 hour fast or a 16 hour fast followed by a 2 hour refeed with normal chow. Livers were homogenized using a dounce homogenizer in 10 mM Tris pH 7.5, 2 mM MgCl₂, 3 mM CaCl₂, 2 U/mL Superase-In and then filtered through a 100 μ m cell strainer to isolate nuclei. Samples were centrifuged at 400 g for 10 minutes and resuspended in the same buffer as above with 10% glycerol and 1% Igepal C-630 to a concentration of about 10^8 nuclei/mL.

For nuclear run-on, about 4×10^7 nuclei were mixed with an equal volume of 10 mM Tris pH 8.0, 5 mM MgCl₂, 1 mM DTT, 300 mM KCl, 200 U/mL Superase-In, 1% sarkosyl, 500 μ M ATP, GTP and Br-UTP, 2 μ M CTP. RNA was extracted from the nuclei using TRIzol and then treated with DNase. Nascent transcripts were immunoprecipitated out of solution using anti-BrdU agarose beads. After elution, the RNA was precipitated with 300 mM NaCl, 20 μ g glycogen, and 2.5 volumes of ethanol and incubated overnight at -20°C . The RNA pellets were resuspended in water (with 1U/ μ L Superase-In and 0.05% Tween 20), denatured for 3 minutes at 65°C , and treated with poly(A)-polymerase for 30 minutes at 37°C .

cDNA was synthesized from the RNA using oNTI223 primer as in ([Wang et al., 2011](#)). 8 μ L of tailed RNA was mixed with 1 μ L dNTP (10 mM each) and 2.5 μ L (12.5 μ M) oNTI223. The samples were heated at 75°C for 3 minutes and chilled on ice. 0.5 μ L Superase-In, 3 μ L 0.1 M DTT, 2 μ L 25 mM MgCl₂, 2 μ L 10x reverse transcription buffer, and 1 μ L superscript III reverse transcriptase were added to the tube. The tube was then incubated for 30 minutes at 48°C . 4 μ L exonuclease I was added to the reaction and the sample was incubated for 1 hour at 37°C to remove excess oNTI223. RNA was eliminated by adding 1.8 μ L of 1 M NaOH and incubating for 20 minutes at 98°C . The cDNA products were recovered by running on a 10% polyacrylamide TBE-urea gel, excising the products from 105–400 bp, and then dissolving the gel in TE with 0.1% Tween-20 for 4 hours. DNA was recovered by adding 20 μ g glycogen and 300 mM NaCl and 2 volumes of ethanol and precipitating overnight at -20°C .

cDNA was resuspended and circularized with CirLigase for 1 hour at 60°C . The sample was then denatured for 10 minutes at 80°C and relinearized by adding 25 mM KCl, 500 μ M DTT and 15 units of APE I. Linearized DNA was amplified via PCR with Phusion polymerase with primers oNTI200 and oNTI201. The PCR product

was run on a 10% TBE gel and products between 150 and 305 nucleotides were excised and the gel was dissolved in TE + 0.1% Tween +150 mM NaCl for 4 hours.

GRO-seq reads were cleaned up by trimming off low-quality base, adaptor, and poly-A tail sequences using cutadapt (Martin, 2011). Trimmed reads with length \geq 25 bp were aligned to UCSC mm9 using Bowtie (Langmead et al., 2009) with an option '-best-strata -m 1 -v 3'. Reads within highly abundant signal regions (such as ribosomal RNA, small nucleolar RNA, small nuclear RNA, and transfer RNA) were removed before downstream analysis to minimize read-depth bias. RPM-normalized bigwig files were generated in a strand-specific manner, where all reads were extended to 150 bp toward 3'-ends for smooth profile. Minus-stranded signals were presented as negative values. GRO-seq bigwig files were visualized using the Integrative Genomics Viewer (IGV) (Robinson et al., 2011). Gene body transcription levels were quantitated in all biological replicates and conditions for comparative analysis. First, all reads were extended to 50 bp towards the 3'-end, then RPKM-normalized read counts were measured within gene bodies excluding the 500 bp region at the 5' end using Gencode (Harrow et al., 2006) annotation. For genes with total gene length < 1 kb, the entire gene body was used. Differential expression analysis was performed comparing Fasted versus Refed mice using EdgeR (Robinson et al., 2010). Genes with FDR <0.05 and >1 RPKM were selected as feeding-dependently regulated genes and were subjected to gene ontology analysis using Enrichr (Chen et al., 2013; Kuleshov et al., 2016; Xie et al., 2021). Hierarchical clustering was performed on the list of feeding-regulated genes generated for gene ontology analysis using WT fast, WT refed, L-AktDKO refed, L-AktFoxo1TKO refed samples. Separate clustering was performed on only the lncRNAs from these samples. Complete-linkage clustering was performed on these transcript levels using Pearson correlation coefficient as a similarity measure. For eRNA analysis, we identified eRNA peaks across all conditions as described previously (Emmett et al., 2017). Briefly, candidate peaks for each condition were filtered against the background in a 10 kb window on either side, with those that passed being pooled together. eRNAs were identified from the pool by searching for paired peaks as many eRNAs are bidirectional. Unpaired peaks that were intergenic or were intragenic but located on the antisense strand of a RefSeq gene were defined as unidirectional eRNAs. For analysis between fasting and refeeding, eRNAs with an RPKM >0.5 in at least one of the conditions were selected and were marked as differentially expressed if the fold-change between conditions was >2 in either direction. Gene ontology for eRNA was done using the Genomic Regions Enrichment of Annotations Tool (GREAT) (McLean et al., 2010) and clustering was performed as it had been for the gene analysis.

mRNA isolation and real-time PCR

Total RNA was isolated from the frozen liver samples using the RNeasy Plus kit from QIAGEN and treated with DNase. Complementary DNA was generated using M-MuLV reverse transcriptase and relative gene expression was quantified by real time PCR using the SYBR Green dye-based assay.

Protein isolation and Western blotting

To isolate protein from the liver, 20-25 mg of tissue was homogenized in RIPA (50mM Tris-HCl, 1% Triton x100, 0.5% Sodium deoxycholate, 0.1% SDS, 150 mM NaCl, 2 mM EDTA) buffer supplemented with protease inhibitor cocktail tablets, and phosphatase inhibitor cocktail II and III in a TissueLyser (QIAGEN). Protein concentrations were determined via the Pierce™ BCA Protein Assay Kit (ThermoFisher). 50 µg of protein were loaded onto and separated by 4%–15% Mini-PROTEAN TGX pre-cast gels. Primary antibodies used were HSP90, Akt2, pAkt2, PRAS40, pPRAS40, and Gck.

Glucose tolerance test

16hr. fasted mice were intra-peritoneally injected with 2 g/kg of glucose in a 20% solution and blood glucose was measured 0, 15, 30, 60, and 120 min post-injection via tail bleed using OneTouch glucose meter and glucose strips.

Serum insulin measurements

Blood was taken from mice via tail bleed after a 16 hour fast and then 15 minutes after intra-peritoneal glucose injection (as during the glucose tolerance test). Serum was separated from the blood by centrifuging the samples for 15 minutes at 5,000 g at 4°C. Insulin concentration was measured from the samples using the Ultra-Sensitive Mouse Insulin ELISA Kit from Crystal Chem.

Primary hepatocyte isolation

Mice were anesthetized w/0.1 g/kg pentobarbital diluted in saline. A midline incision was used to expose the liver. The posterior vena cava was cannulated with a 22g x 1" catheter while the portal vein was cut. The liver was perfused with liver perfusion medium for 4 minutes at a rate of 8 mL/min to exsanguinate it before being perfused with 50 mL of liver digest buffer (Krebs-Ringer bicarbonate buffer with 20 mM HEPES, 500 μ M CaCl₂, 100 U/mL collagenase, and 4.8 U/mL DNase). After digestion, the liver was removed and teased apart in 50 mL of Krebs/HEPES buffer (Krebs-Ringer bicarbonate buffer with 20 mM HEPES) until the liver was completely resuspended. The sample was filtered through a 70-micron cell strainer and then centrifuged at 50 g for 5 minutes at 4°C. The supernatant was removed and the pellet was gently resuspended in 50 mL of a 25% Percoll gradient. The sample was centrifuged again at 120 g for 5 minutes at 4°C and the supernatant was removed. The hepatocyte-containing pellet was washed with Krebs/HEPES buffer and centrifuged again at 120 g for 5 minutes at 4°C and the supernatant was removed. Cells were resuspended in M199 media containing 5 mM glucose, 10% FBS, 500 nM dexamethasone, and 1 nM insulin and plated on 6-well collagen-coated plates for 4 hours to attach at a cell density of 1 million viable cells/well (determined by Trypan Blue staining and counted on a hemocytometer). After attachment, cells were changed to M199 media containing 5 mM glucose and 500 nM dexamethasone and incubated overnight. Cells were switched to M199 containing 5 mM glucose, 10% fetal bovine serum, and 500 nM dexamethasone supplemented with 100 nM insulin and 10 μ M MK2206 per condition. Cells were harvested after 7 hours.

Polysome profiling

200 mg of frozen liver tissue was placed in 1 mL of buffer (100 mM KCl, 5 mM MgCl₂, 10 mM HEPES, 0.5% Igepal C-630 w/100 μ g/mL cycloheximide, 40 U/mL RNaseOut, and 1 \times protease inhibitor added immediately before experiment). Samples were homogenized in a dounce homogenizer with 10 strokes of the loose dounce followed by 10 strokes of the tight dounce. Samples were centrifuged for 5 minutes at 2,000 g at 4°C to remove cellular debris. Supernatant was transferred to a fresh tube and centrifuged again, this time at 12,000 g for 5 minutes at 4°C to remove any remaining debris. RNA content in each sample was measured via OD_{260 nm}. Equal amounts of RNA were loaded onto 10% - 50% sucrose gradients. The loaded samples were centrifuged at 35,000 g for 2.5 hours. After centrifugation, samples were moved to a fractionator and collected in 12 fractions. OD_{260 nm} was measured as fractions were collected to build the profile. Lastly, RNA was extracted from each fraction by adding 1 volume of TRIzol and then a volume of chloroform was added equal to one-fifth the volume of TRIzol. Samples were centrifuged at 2,000 g for 20 minutes. The upper layer was transferred to a fresh tube and 1 volume of 70% ethanol was added. The sample was loaded onto a Qiagen RNeasy spin column and purified following the manufacturer's instructions.

QUANTIFICATION AND STATISTICAL ANALYSIS

Statistical analysis was performed using One-way ANOVA coupled with Tukey's multiple comparison test when more than two groups were compared, Two-way ANOVA with Tukey's multiple comparison test when two conditions were analyzed, and unpaired two-tailed Students' t-test when only two groups were being compared. All data are presented as mean \pm standard error of mean. */† indicates p-value < 0.05, **/†† indicates p-value < 0.01, ***/††† indicates p-value < 0.001, and **** indicates p-value < 0.0001.